Chemistry–A European Journal
Full Paper
doi.org/10.1002/chem.202101032
Chemistry Europe
European Chemical Societies Publishing

Tailoring Valence Tautomerism by Using Redox Potentials: Studies on Ferrocene-Based Triarylmethylium Dyes with Electron-Poor Fluorenylium and Thioxanthylium Acceptors

Larissa A. Casper,[a] Michael Linseis,[a] Serhiy Demeshko,[b] Mykhailo Azarkh,[a] Malte Drescher,[a] and Rainer F. Winter*[a]

Dedicated to Professor Heinrich Lang on the occasion of his 65th birthday

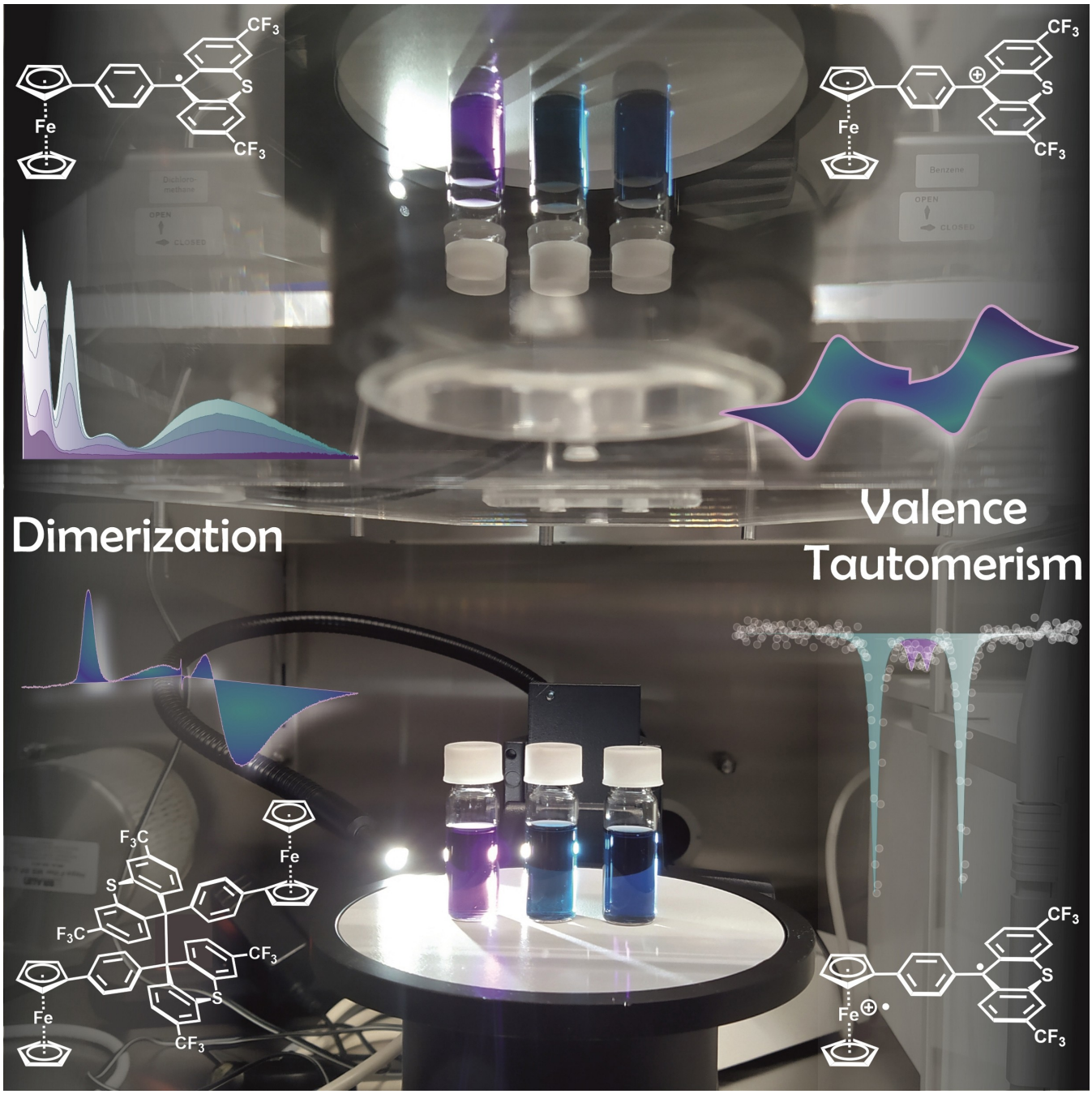

Abstract: Three new electrochromic ferrocenyl triarylmethylium dyes with fluorenylium (**1a**$^+$, **1b**$^+$) or thioxanthylium (**1c**$^+$) residues were selected in order to keep the intrinsic differences of redox potentials for ferrocene oxidation and triarylmethylium reduction small and to trigger valence tautomerism (VT). UV/Vis/NIR and quantitative EPR spectroscopy identified paramagnetic diradical isomers **1a**$^{\bullet\bullet+}$–**1c**$^{\bullet\bullet+}$ alongside diamagnetic forms **1a**$^+$–**1c**$^+$, which renders these complexes magnetochemical switches. The diradical forms **1a**$^{\bullet\bullet+}$–**1c**$^{\bullet\bullet+}$ as well as the one-electron-reduced triarylmethyl forms of the complexes were found to dimerize in solution. For radical **1a**$^\bullet$, dimerization occurs on the timescale of cyclic voltammetry; this allowed us to determine the kinetics and equilibrium constant for this process by digital simulation. Mößbauer spectroscopy indicated that **1a**$^+$ and **1b**$^+$ retain VT even in the solid state. UV/Vis/NIR spectroelectrochemistry revealed the poly-electrochromic behaviour of these complexes by establishing the distinctly different electronic absorption profiles of the corresponding oxidized and reduced forms.

Introduction

The thrive to miniaturize electronic devices sparked an ever-increasing interest in molecular electronics[1] and triggered a boost in the fields of molecular magnetism and molecular spintronics.[1a] From a coordination chemist's viewpoint, a metal-radical approach to molecular magnetism is particularly attractive.[2] This holds in particular for electronically bistable materials whose properties are subject to external stimuli.[3] Molecular magnetic switches[4] and bistable molecular nanomagnets are considered hot candidates for advanced information data storage and processing.[5] One class of compounds showing such properties are metal complexes that exist as two (or more) equilibrating electronic isomers (valence tautomers, VTs),[6] while other compounds may show even more subtle distinctions between two different, coexisting electronic ground states.[7]

VTs classically differ with respect to the oxidation state (i.e., the internal spin and charge) distributions between a redox-active metal ion, typically a 3d element, as the coordination centre and a likewise redox-active, "non-innocent" ligand.[2a,b,8] Owing to their different electronic structures, individual VTs show distinct optical and magnetic properties.[3] Complexes that engage in valence tautomeric equilibria have thus been proposed as candidates for molecular electronic switches ever since their discovery in the 1980s.[8,9] External inputs that can be employed to shift the equilibria are light irradiation,[10] as well as pressure[11] or temperature changes[2b,12] as the most commonly employed external perturbations. The critical temperature T_c defines the point at which equal amounts of both VTs are present in a thermally equilibrated sample.[3]

Scheme 1 provides an overview of some complexes with relevance to the field of valence tautomerism (VT). Classical examples are diimine complexes of 3d metal ions such as

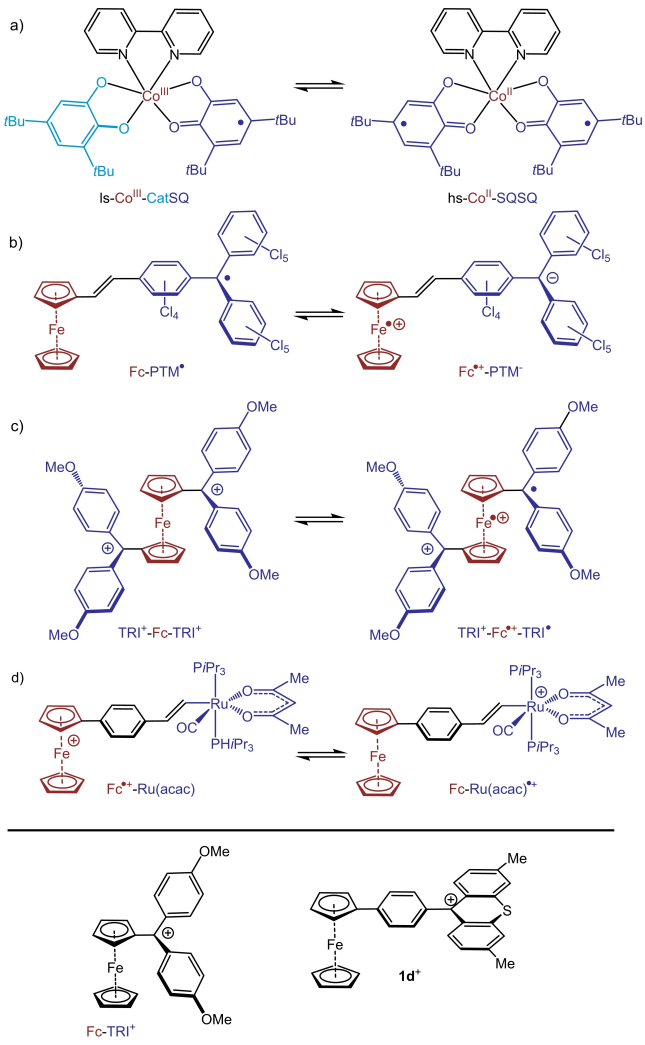

Scheme 1. Valence tautomeric complexes known from the literature and triaryl-methylium-substituted ferrocenes Fc-TRI$^+$ and **1d**$^+$.

[a] *L. A. Casper, Dr. M. Linseis, Dr. M. Azarkh, Prof. M. Drescher, Prof. R. F. Winter*
Fachbereich Chemie, Universität Konstanz
Universitätsstraße 10, 78457 Konstanz (Germany)
E-mail: rainer.winter@uni-konstanz.de

[b] *Dr. S. Demeshko*
Institut für Anorganische Chemie
Georg-August-Universität Göttingen
Tammannstraße 4, 37077 Göttingen (Germany)

Supporting information for this article is available on the WWW under https://doi.org/10.1002/chem.202101032

cobalt,[10–13] copper,[14] nickel,[4] iron,[15] and manganese[6b,16] with dioxolene ligands derived from *o*-quinones and their one- or two-electron-reduced forms, the semiquinonates $SQ^{\bullet-}$ and catecholates Cat^{2-} (Scheme 1 a). Variations of the kind of the diimine and the dioxolene ligands and their substituents offer ample opportunities to fine-tune the equilibria between the individual VTs. Other, recent work centres on a cobalt complex with two terpy-like verdazyl ligands and two-dimensional coordination polymers with a manganese nitronyl nitroxide radical as the active component.[17] Of particular relevance to the present work are the ferrocene-polychlorotriphenylmethyl dyads pioneered by the *Veciana* group, where a ferrocene polychlorotriphenylmethyl radical Fc-PTM$^{\bullet}$ coexists with a zwitterionic ferrocenium-polychlorotriphenylmethanide ($Fc^{\bullet+}$-PTM^{-}) species (Scheme 1 b). These equilibria were thoroughly studied in solution and in the solid state.[18] The latter systems emphasize the general utility of ferrocenes as oxidizible electron donors and reducible triarylmethane-derived acceptors for such purposes. As the Ar_3C scaffold offers three different, accessible charge states, ranging from cations CAr_3^{+} to anions CAr_3^{-},[19] one can also conceive to employ a suitable triarylmethylium cation as the acceptor unit in such ferrocene-CAr_3^{n+} (n = 0, 1) donor-acceptor dyads. The latter approach would then connect diamagnetic ferrocene-triarylmethylium (Fc-CAr_3^{+}) and paramagnetic ferrocenium-triarylmethyl diradicals $Fc^{\bullet+}$-$CAr_3^{\bullet}$ in valence tautomeric equilibria. This would render such systems magnetochemical switches. In first forays towards this aim we have studied some ferrocenyl tritylium cations such as the methoxy-substituted derivative Fc-TRI^{+} on the bottom left of Scheme 1 as well as related 1,1′-bis(tritylium) derivatives, exemplified by the bis(di-*p*-anisyl) congener denoted as TRI^{+}-Fc-TRI^{+} (Scheme 1 c). While monosubstituted Fc-TRI^{+} did not show any signs of VT,[20] variable temperature EPR spectroscopy provided first evidence that extremely electron-poor TRI^{+}-Fc-TRI^{+} coexists with its TRI^{+}-$Fc^{\bullet+}$-TRI$^{\bullet}$ diradical form.[21] The ferrocenyl thioxanthylium complex **1 d**$^{+}$ (Scheme 1, bottom right), where a phenylene spacer separates the ferrocene donor from the methylium centre, also showed a weak EPR signal, pointing to the presence of a minor fraction of a diradical valence tautomer.[22]

Individual VTs interconvert *via* an intramolecular electron transfer between their redox-active subunits. To be considered true VTs, every individual isomer must represent one of two (or more) nearly degenerate electronic states with mutually localized electronic structures.[2b,9a] This translates into a double (multiple) minimum ground-state potential hypersurface, where i) the vertical offset between the different minima ΔG is sufficiently small to allow the different forms to coexist in a thermal equilibrium at reasonable T, and ii) the energy barrier ΔG^{*}, which interconnects individual minima, is sufficiently high to electronically decouple the individual redox sites and to prevent electron delocalization (note that, in the case of a too low energy barrier, the system would collapse into an electronically moderately coupled asymmetric mixed-valent compound, Scheme 2).[9a,23]

Despite the wealth of VTs described in the literature, the purposeful design of compounds exhibiting this phenomenon still poses a challenge. Even minor variations of the connecting spacer or the intrinsic redox potentials of the individual redox sites may tip the scale towards mixed valency or increase ΔG or ΔG^{*} by such a margin that only one isomer can be observed. Examples that demonstrate this delicate balance are provided by the one-electron oxidized forms of ferrocenyl-styrylruthenium complexes of type d in Scheme 1. The shown complex with an acetylacetonate (acac) and related β-ketoenolato complexes with 4-substituted phenyl groups instead of Me exist as two distinguishable valence tautomers.[24] When the acac co-ligand is however replaced by its bis-CF_3 derivative hfac or by the simple chloro ligand, only the isomer with an oxidized ferrocenium centre is present. Removing the phenylene spacer finally leads to an asymmetric mixed-valent description.[25]

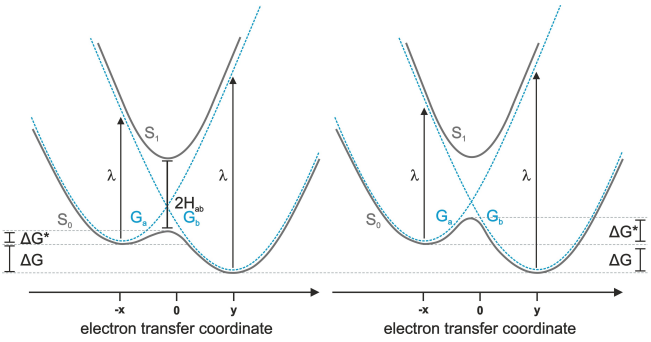

Scheme 2. Potential energy hypersurfaces for an asymmetric mixed-valent compound (left) and a system potentially showing VT (right), depending on the energy difference ΔG and the energy barrier ΔG^{*}.

Our previous results prompted us to employ the general motif of Fc-TRI^{+} in our quest for ferrocene-triarylmethylium species capable of serving as valence tautomeric magnetochemical switches. When considering compound **1 d**$^{+}$ and Scheme 2, it becomes clear that i) the phenylene spacer provides sufficient electronic decoupling between the ferrocene and triarylmethylium redox systems (i.e., ΔG^{*} is sufficiently high), and ii) the inherent difference in redox potentials for ferrocene oxidation and reduction of the 9-phenylthioxanthylium substituent of **1 d**$^{+}$ is just about small enough to render ΔG in a useful range to observe both VTs at convenient temperatures. The modifications discussed herein are substituting the Me groups at the thioxanthylium scaffold for CF_3 and replacing the thioxanthylium with a fluorenylium acceptor. Both these alterations were conceived with the aim of further reducing ΔG.

Results and Discussion

Identifying suitable candidates

The three new ferrocenyl triarylmethylium-derived complexes **1 a**$^{+}$–**1 c**$^{+}$ in this work (cf. Scheme 3) were purposefully chosen with the aim of increasing their propensity to exhibit valence tautomerism (VT). In order to identify promising candidates, we

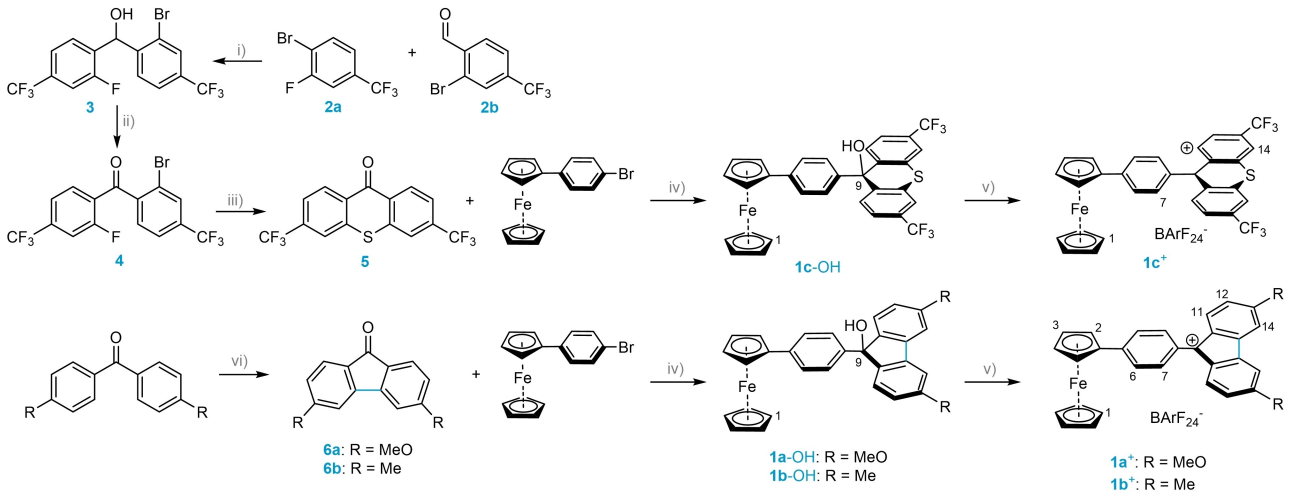

Scheme 3. Synthesis of the ketone (**5**, **6a**, **6b**) and carbinol (**1a**-OH to **1c**-OH) precursors and the target cationic complexes **1a**$^+$-**1c**$^+$ with $[BArF_{24}]^-$ ($[B\{C_6H_3(CF_3)_2\}_4]^-$) as the counterion. i) *n*BuLi in Et_2O, −78 °C, 20 min; ii) PCC in CH_2Cl_2/Celite, RT, 2 h; iii) $Na_2S{\cdot}9H_2O$ in DMF, 85 °C, 5 d; iv) *t*BuLi in THF, −78 °C (3 h), RT (12 h), 60 °C (5 h); v) Brookhart's acid $[H(OEt_2)_2]^+$ $[B\{C_6H_3(CF_3)_2\}_4]^-$ in CH_2Cl_2, RT (1 h); vi) $Pd(OAc)_2$, Ag_2O, K_2CO_3 in TFA, 140 °C, 48 h.[33]

compared the first reduction potentials $E_{1/2}^{+/0}$ of variously substituted triarylmethylium ions to the oxidation potential of ferrocene. As most literature data for substituted triarylmethylium ions are reported relative to the parent triphenylmethylium (tritylium) ion Ph_3C^+, we used its $E_{1/2}^{+/0}$ of −240 mV (in CH_2Cl_2/0.1 M NBu_4^+ $[BF_4]^-$)[26] *versus* the ferrocene/ferrocenium standard couple $Cp_2Fe^{0/+}$ ($E_{1/2}^{0/+} = 0$ mV) for estimating their redox potentials. For those triarylmethylium ions, whose redox potentials are presently not known, we employed the correlation of Strohbusch for *para*-substituted tritylium ions of the type $PhC^+(C_6H_4\text{-}4R)_2$ [Eq. (1)] in order to estimate substituent effects as expressed by their Hammett σ_x^+ constants[19a,27] on $E_{1/2}^{+/0}$ of the corresponding, parent triarylmethylium ion.[28] Comparisons of estimated and experimental $E_{1/2}^{+/0}$ values for other derivatives suggest that this estimate is accurate within a margin of ±25 mV.

$$E_{1/2}^{+/0} = 2\rho \cdot \sigma_x^+ + C = 0.494 \cdot \sigma_x^+ + 0.308\,\text{V}$$
$$\text{with } \sigma_x^+(\text{Me}) = -0.311\,\text{V},\ \sigma_x^+(\text{OMe}) = -0.778\,\text{V},\quad (1)$$
$$\text{and } \sigma_x^+(CF_3) = +0.612\,\text{V}.$$

Table 1 lists the $E_{1/2}^{+/0}$ values for the parent and *para*-disubstituted tritylium, 9-phenyl-fluorenylium and 9-phenyl-thioxanthylium ions with methoxy, methyl or trifluoromethyl substituents. With reduction potentials in the range of +40 mV to −210 mV, the dimethyl-substituted 9-phenyl-fluorenylium ion $Ph(p\text{-}^{Me}FLU)^+$, its dimethoxy-substituted congener $Ph(p\text{-}^{MeO}FLU)^+$, and the trifluoromethyl-substituted 9-phenyl-thioxanthylium $Ph(p\text{-}^{CF3}SXant)^+$ ions were chosen as the most promising candidates.

Table 1. Electrochemical data for unsubstituted triarylmethylium cations from literature and estimated data for substituted 9-phenyl-fluorenylium and 9-phenyl-thioxanthylium ions in mV.

$E_{1/2}^{+/\bullet}$	Ph_3C^+ −240[a]	$Ph(p\text{-}^{Me}C_6H_4)_2^+$ −380[c]	$Ph(p\text{-}^{MeO}C_6H_4)_2^+$ −610[c]
$E_{1/2}^{+/\bullet}$	$PhFLU^+$ +160[b]	$Ph(p\text{-}^{Me}FLU)^+$ +40[c]	$Ph(p\text{-}^{MeO}FLU)^+$ −210[c]
$E_{1/2}^{+/\bullet}$	$PhSXant^+$ −355[d]	$Ph(p\text{-}^{CF3}SXant)^+$ −43[c]	$Ph(p\text{-}^{Me}SXant)^+$ −495[c]

[a] Literature value from ref. [26] in $CH_2Cl_2/NBu_4^+[BF_4]^-$ vs. $Cp_2Fe^{0/+}$. [b] Literature value from ref. [29] in DME/ 0.2 M $LiClO_4$. [c] Estimated value by using equation **1**. [d] Original literature value from ref. [30] in DMSO/ $NBu_4^+[PF_6]^-$.

Synthesis and characterization

The ferrocene-triarylmethylium dyads of our previous studies were conveniently generated from their carbinol precursors and Brookhart's acid,[31] which provides the very weakly coordinating $[B\{C_6H_3(CF_3)_2\}_4]^-$ ($[BArF_{24}]^-$) counterion.[32] The latter was found to be crucial in order to stabilize these strong electrophiles.[20–22] The carbinol precursors **1a**-OH to **1c**-OH were synthesized from 4-ferrocenylphenyl lithium and the respective fluorenone derivatives **6a**, **6b**[33] or the previously unknown 3,6-bis (trifluoromethyl)-9*H*-thioxanthen-9-one, (**5**) according to Scheme 3. Compound **5** was prepared by adopting Kobayashi's method[34] via a three-step synthesis involving nucleophilic attack of the lithiated arene **2a** on benzaldehyde **2b** (see the cautionary note in the Experimental Section), oxidation with pyridinium chlorochromate (PCC), and nucleophilic substitution of the remaining F and Br substituents with simultaneous introduction of the thioether bridge using Na_2S nonahydrate. Synthetic details and spectroscopic characterization of isolated intermediates can be found in the Experimental Section (see the Supporting Information). The resulting carbinols are air-

stable, orange solids and are readily characterized by mass spectrometry as well as by NMR spectroscopy. Selected chemical shifts can be found in Table 2 while full spectra are given as Figures S1–S9 of the Supporting Information.

Successful formation of the target ferrocene-triarylmethylium complexes is indicated by an instantaneous colour change from orange to intense eggplant-violet (**1a**$^+$), turquoise (**1b**$^+$) or dark blue (**1c**$^+$, cf. Figure 4, left) on addition of equimolar amounts of Brookhart's acid.[31] Following the reaction by cyclic voltammetry (CV) indicated that the oxidation wave of the respective carbinol is replaced by those of the corresponding dyad within 1 min (vide infra). Mass spectrometry (ESI-MS) readily identified the cations **1a**$^+$–**1c**$^+$ (cf. Experimental Section in the Supporting Information, Figures S10–S12). Spectroscopic characterization of **1a**$^+$–**1c**$^+$ by NMR spectroscopy was, however, partially thwarted by severe paramagnetic broadening of particularly the resonance signals of the protons at the ferrocene nucleus and of protons H11 in direct vicinity to the methylium centre (Scheme 4). Nevertheless, useful ^{1}H{^{13}C} NMR spectra could be recorded in CD_2Cl_2 solutions for sample concentrations of 17–32 mM (Figures 1 and S13–S21). Paramagnetic broadening and the instability of particularly the fluorenylium compounds **1a**$^+$ and **1b**$^+$ in solution precluded us, however, from recording meaningful ^{13}C NMR spectra. Despite careful handling, dissolved samples of **1a**$^+$ to **1c**$^+$ showed clear signs of decomposition into diamagnetic products within 24 hours with significant discoloration. Some decomposition is even noted on storing solid samples under inert atmosphere at −20 °C for several days. This instability is likely due to an inherent reactivity of their diradical valence tautomers (vide infra) towards oxygen,[21,35] or to hydrogen or chlorine atom abstraction from the solvent. In order to obtain reproducible results, it was therefore mandatory to prepare samples of all complexes freshly in a nitrogen-filled glovebox before every measurement for the entirety of all further studies.

Table 2. Selected ^{1}H NMR data for the ferrocenyl triarylmethylium ions and their carbinol precursors.

	δ_{H1} (1$^+$/1-OH)	δ_{H2} (1$^+$/1-OH)	δ_{H3} (1$^+$/1-OH)	δ_{H7} (1$^+$/1-OH)	δ_{H11} (1$^+$/1-OH)
1a	4.99/4.01	5.87/4.59	5.52/4.28	6.90/7.27	7.10/7.23
1b	4.54/4.01	6.05/4.57	5.58/4.27	n.a.[a]/7.30	n.a.[a]/7.25
1c	4.34[a]/3.98	5.06/4.56	4.91/4.29	6.03[b]/6.77	8.21[b]/8.27
1d[c]	4.23/3.98	4.92/4.54	4.59/4.26	7.39/7.27	8.26/7.88

[a] Chemical shift could not be accurately determined due to the absence or strong broadening of the signal. [b] Assignment based on comparison to the carbinol precursor, as no 2D NMR spectra could be recorded. [c] Values from ref. [22].

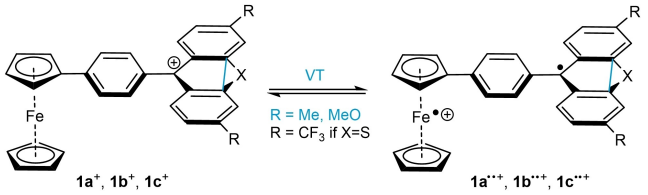

Scheme 4. Valence tautomeric equilibrium between the two redox isomers **1a**$^+$-**1c**$^+$ (left) and **1a**$^{\bullet\bullet+}$-**1c**$^{\bullet\bullet+}$ (right).

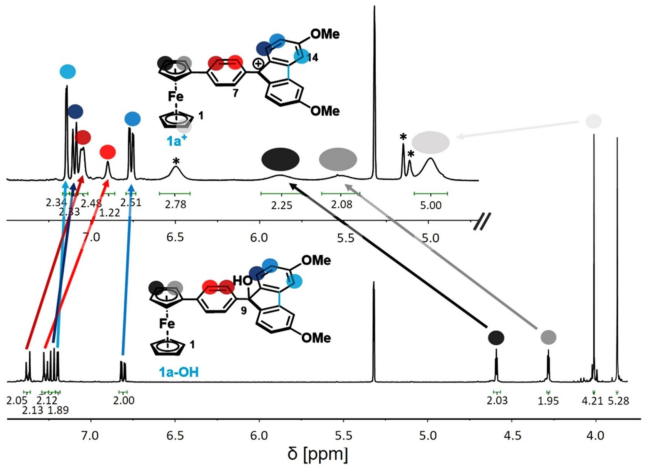

Figure 1. Excerpt of the aromatic and ferrocenyl protons of ^{1}H NMR spectra of complexes **1a**$^+$ (top) and **1a**-OH (bottom) in CD_2Cl_2.

Figure 1 compares the ^{1}H NMR spectra of cation **1a**$^+$ and its carbinol precursor **1a**-OH. The most pertinent shift data of all complex pairs are collected in Table 2. It becomes immediately apparent that paramagnetic broadening affects primarily the ferrocenyl protons and those at the phenylene linker (red marks in Figure 1), while other resonances remain sharp. This is exemplified by the signals of fluorenylium protons H12 and H14 (light blue marks in Figure 1), for which even the characteristically small $^4J_{HH}$ coupling constant of 2.17 Hz can be clearly observed. The latter protons also exhibit only minor shifts to higher fields on conversion of the carbinols to the ferrocenyltriarylmethylium dyads. In contrast, the ferrocenyl protons are strongly displaced to lower field, by up to 1 ppm for protons H1 at the unsubstituted, and by up to 1.48 ppm for protons H2/H3 at the substituted Cp deck. This already suggests that a certain fraction of the cationic complexes exist as their diradical VTs **1a**$^{\bullet\bullet+}$ to **1c**$^{\bullet\bullet+}$ (Scheme 4) or their C–C-coupled dimers (vide infra), which all feature paramagnetic ferrocenium entities. The broadening and sizable upfield shifts of the phenylene resonances show that the unpaired spin density is delocalized onto the adjacent phenylene linker.

In agreement with their paramagnetically broadened NMR resonances, pristine cations **1a**$^+$–**1c**$^+$ are EPR active in fluid solution and give rise to structured EPR signals with resolved hyperfine couplings to protons at the fluorenyl or thioxanthyl scaffold (note that under these conditions, no EPR signatures of the ferrocenium constituent can be observed). A detailed discussion of the EPR spectra and the lessons to be learned from them is deferred to a later section of this paper. For now, it is sufficient to say that the observed EPR activity further supports the relevance of the valence tautomeric equilibria of Scheme 4. The absence of a broadening or suspicious shifting of the ^{1}H NMR resonances at the diarylmethylium unit is initially puzzling. However, fluorenyl radicals are known to engage in monomer-dimer equilibria, which leads to (partial) spin cancel-

lation due to formation of a dynamic covalent bond.[36] In the present context, this means that any diradical VT will coexist with its dicationic dimer, where only the unpaired spins at the ferrocenium subunits remain. Indeed, our EPR study discussed later in this work shows that the vast majority of the diradical VTs exist as dimers. The observation of $[M_2]^{2+}$ peaks in the mass spectra of complexes **1a**$^+$ and **1b**$^+$ provide further indication as to the presence of such dimers (cf. Figure 6, top left and Figures S10–S11, for example, peaks at *m/z* 453.147, 100%; 453.647, 67%; calcd. for $^{\bullet+}$**1b**–**1b**$^{\bullet+}$: *m/z* 453.130, 100%; 453.632, 67%). Extensive delocalization of the unpaired spin density at the triarylmethyl entity of the corresponding monomeric species may also contribute to the absence of paramagnetic broadening. As listed for compound **1a** in Table 3, the DFT calculated Mulliken spin densities for the **1a**$^{\bullet\bullet+}$ valence tautomer and one-electron-reduced **1a**$^{\bullet}$ are delocalized over the methyl centre, the attached aryl rings and, less so, over the phenylene connector. The major difference between the **1a**$^{\bullet\bullet+}$ diradical VT and reduced **1a**$^{\bullet}$ is the presence of the additional ferrocenium-based spin in the former.

Electrochemistry

The differences $\Delta E_{1/2}$ between the half-wave potentials for ferrocene oxidation and triarylmethylium reduction within a dyad **1a**$^+$–**1c**$^+$ provide an estimate of the energy differences between the individual VTs and hence the propensity for exhibiting valence tautomerism. With this in mind, we recorded cyclic voltammograms of complexes **1a**$^+$–**1c**$^+$ and their carbinol precursors **1a**-OH to **1c**-OH in the very weakly nucleophilic CH_2Cl_2/0.1 M NBu_4^+ $[BArF_{24}]^-$ electrolyte. The results are listed in Table 4.

As shown in Figure S22, carbinols **1a**-OH to **1c**-OH as well as the previously reported **1d**-OH[22] show the expected reversible one-electron oxidation of the ferrocene nucleus. The associated half-wave potentials $E_{1/2}^{0/+}$ fall in a narrow range of 80 to 135 mV (cf. Table 4), indicating that these carbinols are less electron-rich than parent ferrocene or phenylferrocene ($E_{1/2}^{0/+} = 25$ mV in CH_2Cl_2/NBu_4^+ $[PF_6]^-$).[37] The small influence of the different kinds of diarylmethyl pendants and their substituents (Me/MeO (**1a/1b**); CF_3/Me (**1c/1d**)) results from the quaternary, sp^3-hybridized C-OH connector, which cripples conjugation.[20–22]

Figure 2 and Figures S23 to S26 show the voltammograms of the three new ferrocene-triarylmethylium dyads **1a**$^+$–**1c**$^+$ at a scan rate *v* of 100 mV/s. They all feature two redox waves, one for ferrocene oxidation and one for the reduction of the triarylmethylium acceptor. The latter wave is consequently absent in the carbinol precursors. Conversion of the carbinols to the ferrocenyl triarylmethylium dyads shifts the half-wave potential for ferrocene oxidation anodically by 160 mV (**1c**$^+$) to 295 mV (**1a**$^+$). Obviously, the increased acceptor strength of the triarylmethylium unit is transmitted to the ferrocene nucleus *via* the phenylene spacer. One should note that Fc-TRI$^+$ (cf. Scheme 2, bottom left) and TRI$^+$-Fc-TRI$^+$; Scheme 2c), where the ferrocenyl unit is directly connected to the methylium acceptor(s), have much higher oxidation potentials of 830 and 1640 mV, respectively.[20,21] By the same token, replacing the 9-phenyl with the more electron-rich 9-(4-ferrocenyl)phenyl substituent shifts the reduction potential of the respective triarylmethylium acceptor cathodic (negative) by 160 mV to 250 mV (Tables 1 and 4). For **1c**, even the second reduction of the triarylmethylium ion, that is, the **1c**$^{\bullet}$/**1c**$^-$ redox couple,

Table 3. Mulliken spin densities[a] for the diradical VT **1a**$^{\bullet\bullet+}$ and reduced **1a**$^{\bullet}$.

	Ferrocene	Phenylene	*C*(CAr_3)	Aryl subst.	Overall spin
1a$^{\bullet\bullet+}$	1.05	0.07	0.56	0.32	2
1a$^{\bullet}$	0.02	0.07	0.58	0.33	1

[a] Calculated values from DFT; hydrogen atom contributions are summed with those of the C atoms to which they are attached.

Table 4. Electrochemical data[a] for all complexes.

	$E_{1/2}^{ox}$ (ΔE_p)	$E_{1/2}^{red}$ (ΔE_p)	$\Delta E_{1/2}$[b]	$\Delta E_{HOMO/LUMO}$[c]
1a$^+$	260 (75)	−270[d]	ca. 500[g]	2.06
1b$^+$	375 (65)	−40 (80)	415	1.95
1c$^+$	295 (67)	0 (93)	295	1.78
1d$^+$[e]	130 (70)	−665 (77)[f]	795	2.19
1a-OH	80 (65)	n.a.	n.a.	4.68
1b-OH	80 (80)	n.a.	n.a.	4.79
1c-OH	135 (64)	n.a.	n.a.	4.63
1d-OH[e]	95 (73)	n.a.	n.a.	4.98

[a] All potentials in mV (±5 mV) in CH_2Cl_2 / NBu_4^+ $[BArF_{24}]^-$ (0.1 M) at T = 293(±3) K and scan rate v = 100 mV/s relative to the $Cp_2Fe^{0/+}$ redox couple. [b] Half-wave potential separation in mV. [c] From DFT calculations; data in eV. [d] Peak potential of an irreversible redox process. [e] Values from ref. [22] under identical conditions. [f] Second reduction at $E_{1/2}$ = −1270 mV with ΔE_p = 62 mV. [g] Estimated by assuming that the cathodic peak of the reduction wave is ca. 30 mV negative of the half-wave potential of a chemically reversible process, not considering the peak shift arising from the chemical follow step.

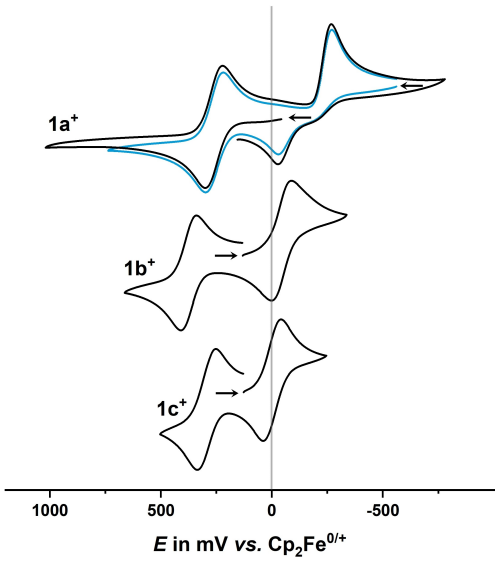

Figure 2. Cyclic voltammograms of **1a**$^+$-**1c**$^+$ (CH_2Cl_2/0.1 mM NBu_4^+ $[BArF_{24}]^-$, 293(±3) K, v = 100 mV/s).

could be observed within the potential window of the CH_2Cl_2/NBu_4^+ $[BArF_{24}]^-$ electrolyte at a half-wave potential of −1270 mV (Figure S23). π-Conjugation between the ferrocene donor and the triarylmethylium acceptor across the phenylene connector hence increases the half-wave potential for ferrocene oxidation, while shifting that of triarylmethylium reduction to more negative values when compared to their simple phenyl-substituted congeners. The potential separation of these processes $\Delta E_{1/2}$ remains nevertheless rather modest. This holds in particular for complex **1c**$^+$, rendering it a particularly promising candidate for observing valence tautomerism.

The reduction of complexes **1b**$^+$ to **1d**$^+$ (Scheme 1, bottom right) constitutes a chemically reversible and an electrochemically quasireversible one-electron process. In contrast, one-electron-reduced **1a**$^\bullet$, the most electron-rich representative of the present complex series, engages in a rapid chemical follow reaction as is indicated by the absence of an anodic counter peak II for the reoxidation of electrogenerated **1a**$^\bullet$. Instead, a new anodic peak, denoted as peak III in Figure 3, is observed. This peak is absent when the cathodic scan is clipped before traversing the primary reduction, peak I in Figure 3.

Assuming the reaction scheme provided in Figure 3, digital simulations successfully reproduced the experimental voltammograms as demonstrated in the top right panel of Figure 3 (see also Figure S27 and Table S2). In Figure 3, electrochemical reactions are portrayed horizontally while chemical conversions are shown in vertical direction. Our simulations confirm that the wave for oxidation/rereduction of the ferrocenyl/ferrocenium constituent (peaks IV/V) exhibits ideal Nernstian behaviour with no sign of chemical side reactions. More importantly, they indicate that reduction to **1a**$^\bullet$ is followed by dimerization to give **1a**–**1a**. The resulting dimer is then reoxidized in two consecutive one-electron steps IIIa and IIIb with close oxidation potentials. It should be noted that, although these oxidations seem to occur as one single wave, assuming a single two-electron process did not provide satisfactory matches between simulated and experimental voltammograms. The one- and two-electron oxidized dimer, in turn, equilibrates with one equivalent of **1a**$^+$ and **1a**$^\bullet$ or with two equivalents of **1a**$^+$. CV simulations for seven different scan rates from 200 to 2000 mV/s provided an estimate for the equilibrium constant K_{dim} for the dimerization of **1a**$^\bullet$. The value of $K_{dim} = 2\times10^5$ L mol^{-1} corresponds to a ΔG value of −29.7 kJ mol^{-1} and indicates that the equilibrium 2 **1a**$^\bullet$ ⇌ **1a**–**1a** is strongly biased towards the dimer.

9-Phenyl-fluorenyl radicals are highly reactive and are generally more prone to dimerization than classical triphenylmethyl (trityl) radicals.[38] The bond dissociation energy of 63.6 kJ mol^{-1}[36,39] of the corresponding dimer is considerably larger than that of ordinary trityl radicals (ranging from 31–39 kJ mol^{-1}[40] depending on the *para* substituents) or that of alkylated derivatives such as hexakis(2,6-di-*tert*-butyl-4-biphenyl)ethane.[41] The latter adopt genuine hexaphenylethane instead of the more common quinoid 4-methylene-2,5-cyclohexadiene structures (the so-called Jacobson-Nauta structure) of ordinary trityl radicals.[39,42] Underlying reasons are lesser steric repulsion and the smaller resonance stabilization of a 9-phenyl-fluorenyl radical.[38] Indeed, 9-phenyl-fluorenyl radicals are considered prime candidates for dynamic covalent chemistry (DCC).[36,39,43] In contrast, 9-Phenyl-(thio)xanthyl radical dimers are less stable than ordinary trityl radicals.[44] Representatives with a rigid binaphthyl clamp between the carbyl centres have provided significantly elongated C–C bonds of 1.651 Å.[45] The extent of dimerization of the thioxanthyl ferrocenyl radical **1d**$^\bullet$ was nevertheless determined as 97% by quantitative EPR spectroscopy.[22] We also note that the ferrocenyl-substituted triarylmethyl radicals Fc-TRI$^\bullet$ and TRI$^+$-Fc-TRI$^\bullet$ (Scheme 2) were

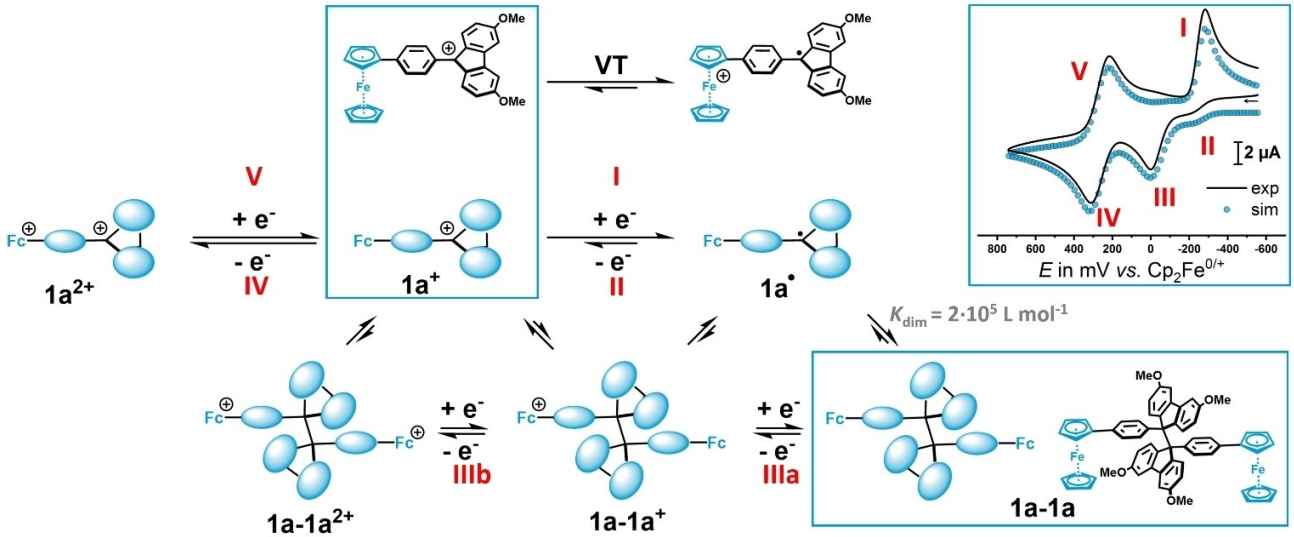

Figure 3. Experimental cyclic voltammogram (top right, black curve) of **1a**$^+$ ($v = 400$ mV s^{-1}) in CH_2Cl_2/NBu_4^+ $[BArF_{24}]^-$ (0.1 M) at $T = 293(\pm3)$ K and the corresponding simulation (blue dots) with the equilibrium constant K_{dim} [L mol^{-1}] and the underlying reaction mechanism. Electrochemical steps are displayed in horizontal and chemical conversions in vertical directions.

found by *T*-dependent EPR spectroscopy to dimerize to a considerable extent.[20–22]

Electronic spectroscopy and spectro-electrochemistry

Compounds **1a**$^+$–**1c**$^+$ are intensively colored, giving violet (**1a**), turquoise (**1b**) or royal blue (**1c**) solutions as shown in Figure 4. Figure 4 also displays the UV/Vis/NIR absorption spectra of the complexes. Pertinent data of the cationic complexes as well as those of their one-electron-reduced and one-electron oxidized forms (vide infra) are compiled in Table 5. TD-DFT calculations identify the visible absorptions in the range of 400 to 600 nm as resulting from the so-called x- and y-bands, resorting to the definition established for tritylium dyes.[46] Contour plots of the molecular orbitals that contribute to the respective transitions of **1b**$^+$ as well as the corresponding TD-DFT computed electron density difference maps (EDDMs) are provided in Figure 5 along with an assignment of the individual

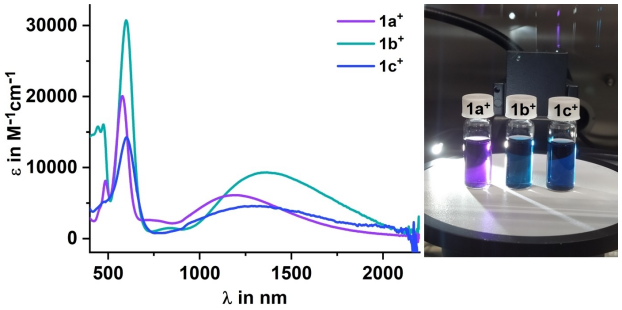

Figure 4. UV/Vis/NIR spectra of complexes **1a**$^+$-**1c**$^+$ in CH_2Cl_2 at $T = 293(\pm 3)$ K with photographs taken inside a nitrogen-filled glovebox.

Table 5. UV/Vis/NIR data[a] for the cationic complexes, computed HOMO/LUMO energies and interplanar angles at the phenylene linker.

	λ [nm] (ε [Lmol^{-1}cm^{-1}])[b]	E_{LUMO}/E_{HOMO}[c]	$\angle_{Cp/Ph}/\angle_{Ph/Trityl}$[c]
1a$^\bullet$	449 (1180)	−4.676/−0.866	−18.1/37.8
1a$^+$	386 (3260), 449 (4200), 484 (8490), 576 (20080), 753 (2720), 1195 (6110)	−6.191/−4.127	−8.5/36.4
1a^{2+}	479 (17260), 778 (3160), 841 (2720)	−7.105/−4.501	−9.8/41.9
1b$^\bullet$	450 (2610)	−4.932/−0.750	−20.2/37.2
1b$^+$	475 (17530), 598 (30890), 845 (4170), 1373 (11580)	−6.307/−4.358	−6.9/34.0
1b^{2+}	356 (26300), 522 (34960), 769 (4590)	−7.450/−4.825	−9.5/39.9
1c$^\bullet$	455 (4450), 545 (5090)	−4.964/−1.227	−22.0/76.7
1c$^+$	475 (5120), 601 (14200), 1299 (4540)	−6.138/−4.360	−11.8/58.1
1c^{2+}	509 (11890), 723 (2340), 765 (2280)	−7.836/−4.665	−21.0/69.5
1d$^+$	405 (28000), 505 (5000), 528 (4000), 743 (1000)	−6.05/−3.86	−20.4/62.1

[a] In 1,2-$C_2H_4Cl_2$/0.25 mM NBu_4^+ $[BArF_{24}]^-$ at 293(±3) K. [b] Absorption coefficients ±10 Lmol^{-1}cm^{-1}. [c] Energies in eV; angles and energies according to DFT calculations with the PBE0 functional on the cationic, the reduced, and the oxidized complexes. Values of the ferrocenium chromophore are shown in light blue.

transitions. Corresponding representations for complexes **1a**$^+$ and **1c**$^+$ can be found in Figures S28 and S29.

The y-band involves charge transfer (CT) from mainly the substituted Cp^- ligand to the LUMO, which is delocalized over the entire triarylmethylium acceptor. The x-band results from an excitation into the same acceptor orbital, but with the aryl rings at the diarylmethylium entity as the donors. Of particular interest is the electronic absorption band at the lowest energy, which is shifted well into the near infra-red (NIR). The latter has no counterpart in ordinary tritylium dyes and is assigned as metal-to-ligand charge transfer (MLCT) from the iron-based HOMO at the ferrocenyl donor to the LUMO (see also Figures S28 and S29). This absorption has consequently been dubbed as the y_M-band.[20,22] We note a generally very satisfactory match between calculated and experimental spectra apart from the fact that the calculations overestimate the band energies, which is a known problem for charge-transfer excitations in TD-DFT (Figure 5, bottom right and Figure S30).[20] The energy at the absorption maximum of the y_M-band decreases in the order **1a**$^+$ > **1c**$^+$ > **1b**$^+$. This ordering does not fully comply with the DFT-computed HOMO-LUMO energy gaps $\Delta E_{LUMO/HOMO}$ (Table 4), but matches with that of the TD-DFT computed transition energies (Figures 5 and S28–S30) and the half-wave potential differences for ferrocene oxidation and triarylmethylium reduction (Table 4). The geometry-optimized structures of the cationic complexes indicate a high degree of coplanarity between the cyclopentadienide ligand and the phenylene linker, but a larger torsion between the phenylene linker and the plane defined by the sp^2 hybridized methylium centre and the directly attached carbon atoms. The latter amounts to about 35° in the fluorenylium complexes **1a**$^+$, **1b**$^+$, and to 58° in the thioxanthylium complex **1c**$^+$. The larger torsion in **1c**$^+$ arises from the closer spatial proximity of the *ortho*-hydrogen atoms at the thioxanthylium residue to those at the phenylene linker due to the presence of a central six-membered ring structure instead of a five-membered one. That rotation also reduces phenylene contributions to the LUMO of **1c**$^+$ and decreases the extinction coefficients of the y- and the y_M-bands with respect to complexes **1a**$^+$ and **1b**$^+$. The differences between **1a**$^+$ and **1b**$^+$ can be traced to enhanced CT to the stronger methylium acceptor in **1b**$^+$.

Their redox-activity and the nature of their electronic transitions render the present complexes electrochromic. This endows them with yet another dimension of switchability, which is generally a desirable asset.[3] In order to probe the electrochromism of our new complexes, we monitored the changes of absorption spectra upon oxidation and one-electron-reduction in a spectro-electrochemical setup. Figure 6 illustrates the results for complex **1a**$^+$; those of the other two complexes can be found as Figures S31 and S32. Pertinent data to the electronic spectra of the corresponding dications and the neutral radicals are also listed in Table 5.

Upon reduction (cf. Figure 6, right), all UV/Vis and NIR bands below 500 nm bleach. This is a foreseeable result as one-electron-reduction removes the electron-accepting properties of the triarylmethylium entity and directly effects the LUMO, which is the common acceptor orbital for all relevant electronic

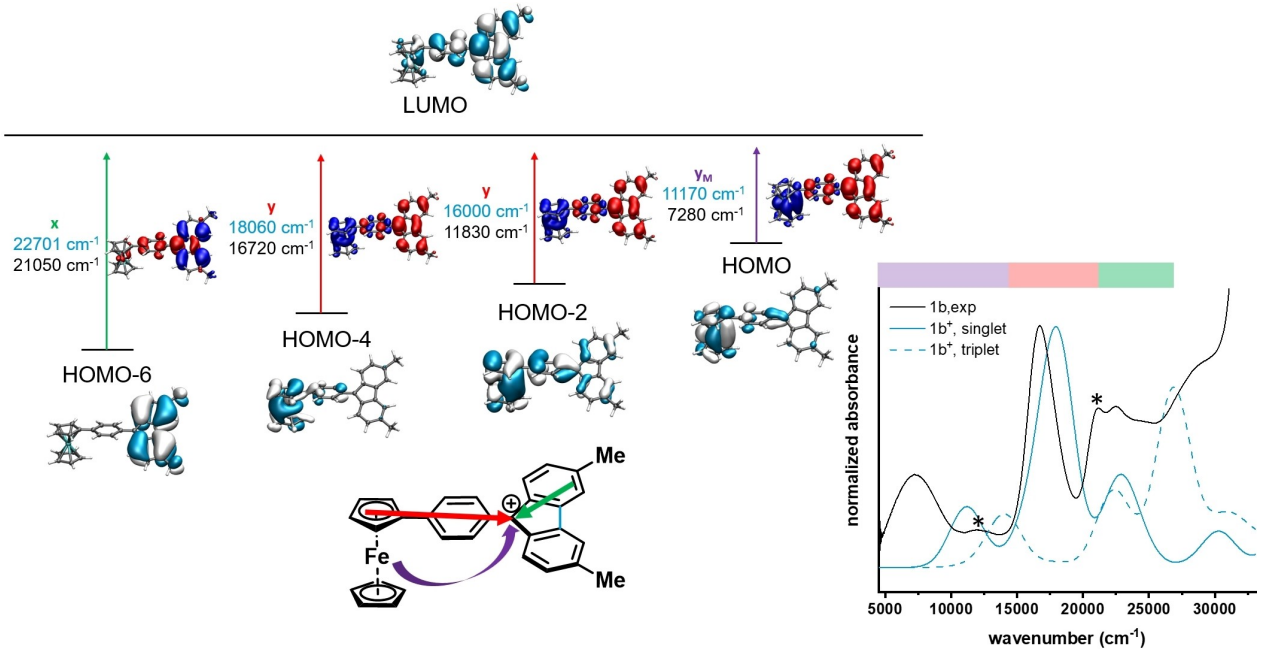

Figure 5. Molecular orbital contributions to the most important transitions of complex $\mathbf{1b}^{+}$ calculated by TD-DFT and the corresponding electron density difference maps (EDDMs). Blue/red colours indicate a loss/gain of electron density. Bottom left: assignment of the individual transitions. Bottom right: comparison of the experimental (black line) and the TD-DFT computed absorption spectra for the singlet (blue solid line) and triplet (blue broken line) states. The asterisks mark "extra" peaks that we assign to the diradical valence tautomer $\mathbf{1b}^{\bullet\bullet+}$.

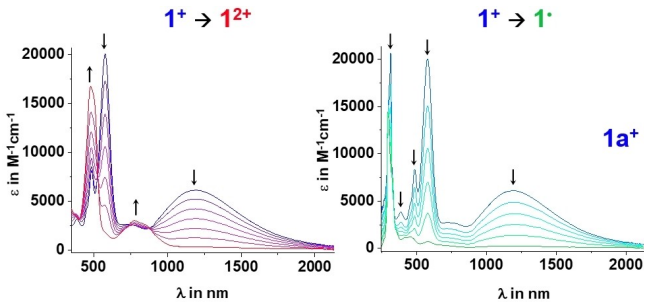

Figure 6. Spectro-electrochemical measurements for $\mathbf{1a}^{+}$ (left: oxidation; right: reduction) in 1,2-$(CH_2)_2Cl_2$ at $T = 293(\pm 3)$ K with 0.1 mM NBu_4^{+} $BArF_{24}^{-}$ electrolyte.

transitions. Spectral changes upon one-electron-reduction are completely reversed on reoxidation, even for complex $\mathbf{1a}^{+}$. This adds further credibility to the chemically reversible monomer/dimer equilibrium of Figure 3. Upon oxidation (cf. Figure 6, left), the bleaching of the y- and y_M-bands is accompanied by the growth of a new, prominent, and hypsochromically shifted y-band (Figures 6, S31 and S32). In addition, a band characteristic of the ferrocenium-type chromophore appears at 723 to 778 nm (values are highlighted by blue coloration in Table 5). The colors of the oxidized species range from burgundy red in the case of $\mathbf{1c}^{2+}$ to Tyrian purple for $\mathbf{1b}^{2+}$ whilst the reduced species $\mathbf{1}^{\bullet}$ appear in different tones (greenish to ochre) of yellow.

In our TD-DFT calculations, we have also considered the possible presence of diradical ferrocenium-trityl valence tautomeric forms $\mathbf{1a}^{\bullet\bullet+}$–$\mathbf{1c}^{\bullet\bullet+}$ in the parent cationic complexes. According to our calculations, this second valence tautomer should display shifted y_M-, y- and x-bands as well as a more intense band below 400 nm than their diamagnetic isomers. Indeed, the UV/Vis spectra of particularly the fluorenylium compounds $\mathbf{1a}^{+}$ and $\mathbf{1b}^{+}$ provide some hints to the presence of such a second isomer such as the weak band near 800 nm (12500 cm^{-1}) or the additional peak in between 440 and 500 nm (20000 to 22500 cm^{-1}; Figures 4 and 5).

In order to further probe for the potential presence of a second electronic isomer in complexes $\mathbf{1a}^{+}$–$\mathbf{1c}^{+}$, we investigated the *T*-dependence of their UV/Vis/NIR spectra over a temperature range of 20 to −70 °C under inert gas atmosphere. In CH_2Cl_2 solutions, compounds $\mathbf{1a}^{+}$ and $\mathbf{1c}^{+}$ showed only minor or no alterations (cf. Figures S33 and S34). However, the spectra of the methyl fluorenylium complex $\mathbf{1b}^{+}$ changed appreciably with temperature, in particular in between −50 and −70 °C (Figure 7, bottom left). The resultant spectroscopic changes resemble those observed during one-electron oxidation or reduction, including the strong bleach of the y_M- and y-bands associated with charge-transfer from the ferrocenyl donor and the appearance of the ferrocenium band at 830 nm. This finding does not only provide further evidence for the presence of variable amounts of the second valence tautomer $\mathbf{1b}^{\bullet\bullet+}$ in samples of $\mathbf{1b}^{+}$, but also suggests that the amount of this valence tautomer increases as *T* is lowered. This contrasts with the behaviour of spin state isomers in coordination chemistry, where the larger entropies of the high spin forms infallibly dictate that the latter are favored at higher *T*, whereas the low-spin forms constitute the enthalpic minimum and

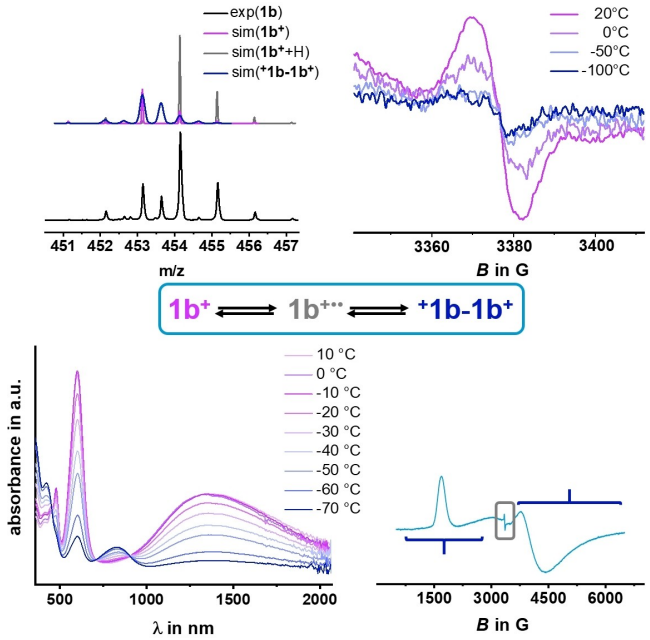

Figure 7. Studies on complex $\mathbf{1b}^+$. Top left: ESI-MS (black) and simulations bottom left: *T*-dependent UV/Vis/NIR spectra; top right: *T*-dependent EPR spectra in CH_2Cl_2; bottom right: EPR spectrum in CH_2Cl_2 at 10 K.

dominate at low *T*. One should however consider that $\mathbf{1b}^{\bullet\bullet+}$, as any other diradical form of this kind (Figure 3), engages in a monomer-dimer equilibrium. The shifting of this equilibrium towards the dimer at lower *T* will therefore also affect the valence tautomeric equilibrium, such that these two processes are strongly intertwined. As previously mentioned, the mass peak of a dicationic dimer was clearly found in the mass spectra of the two fluorenylium complexes $\mathbf{1a}^+$ and $\mathbf{1b}^+$ (cf. Figure 7, top left). We will see in the following section that *T*-dependent EPR spectroscopy provides further evidence that complexes $\mathbf{1a}^+$–$\mathbf{1c}^+$ exist as two equilibrating VTs that engage in monomer/dimer equilibria.

EPR and Mößbauer spectroscopy

This section details the results of our EPR spectroscopic studies. We will first discuss the EPR spectra of the one-electron-reduced forms $\mathbf{1a}^{\bullet}$–$\mathbf{1c}^{\bullet}$. This will be followed by quantitative spin counting at variable *T*, which ultimately provides estimates of the equilibrium quantities present in solutions of the free radicals. In the third step, we will apply EPR spectroscopy to the parent, cationic forms of the complexes in order to gain further insight into the relevance of the paramagnetic VTs $\mathbf{1a}^{\bullet\bullet+}$–$\mathbf{1c}^{\bullet\bullet+}$ and their dimers.

Samples of the neutral radicals $\mathbf{1a}^{\bullet}$–$\mathbf{1c}^{\bullet}$ were readily prepared by reducing their cationic parents with 2.2 equivalents of decamethylferrocene under inert gas atmosphere in CH_2Cl_2. The reducing agent was chosen to effect quantitative conversion ($E_{1/2}^{+/0} = -580$ mV)[47] without interfering with the EPR measurements (note that excess decamethylferrocene as well as the decamethylferrocenium ion are EPR silent under the employed conditions).[48] The reduced complexes $\mathbf{1a}^{\bullet}$–$\mathbf{1c}^{\bullet}$ yield isotropic EPR signals with resolved hyperfine splittings (hfs) to the four sets of nearest protons (Figure S35 and Table S1). Their *g* values are listed in Table 6; they are close to that of 2.003 for ordinary trityl radicals and indicate an organic-centred spin density.[49] The hfs constants in Table S1 were extracted from spectral simulations, which were performed with EasySpin[50] and agree well with the DFT-computed compositions of the diarylmethylium-based LUMOs of the parent cations $\mathbf{1a}^+$–$\mathbf{1c}^+$ and the SOMOs of radicals $\mathbf{1a}^{\bullet}$–$\mathbf{1c}^{\bullet}$ as well as the computed distributions of the unpaired spin densities (see the top panels of Figure 8 for results on the $\mathbf{1c}^+/\mathbf{1c}^{\bullet}$ redox pair and Figure S36 for the other complexes). The latter reside dominantly on the diarylmethyl entities with minor contributions from the phenylene linker.

Next, we recorded *T*-dependent EPR spectra of radicals $\mathbf{1a}^{\bullet}$–$\mathbf{1c}^{\bullet}$ over a *T* range of 20 to −150 °C in (frozen) CH_2Cl_2 in order to obtain further information on their dimerization behaviour. According to the Maxwell-Boltzmann relation of Equation (2), the signal intensity of a free radical is supposed to increase upon cooling due to a higher difference ΔN in occupancy of the ground and the excited states:

Table 6. EPR data and results from quantitative spin-counting experiments on the reduced[a] and cationic[b] complexes.

	g_{iso}	Dimerization [%][c]	Amount of radical monomer [%][c]	Amount of VT [%][d]	$d_{C\text{-}C}$ [Å][e]	Mulliken spin density[f]
$\mathbf{1a}^{\bullet}$	2.0032	99.9 (±0.3)	0.1 (±0.3)	n.a.	1.638	0.91[g]
$\mathbf{1a}^{\bullet\bullet+}$	2.0032	n.a.	n.a.	8.0 (±1.1)	1.602	0.88[g]/1.05[h]/
$\mathbf{1b}^{\bullet}$	2.0041	99.6 (±0.3)	0.4 (±0.3)	n.a.	1.630	0.91[g]
$\mathbf{1b}^{\bullet\bullet+}$	2.0041	n.a.	n.a.	9.0 (±1.0)	1.594	0.89[f]/1.04[h]/
$\mathbf{1c}^{\bullet}$	2.0044	59.0 (±6)	41.0 (±6)	n.a.	1.729	1.02[g]
$\mathbf{1c}^{\bullet\bullet+}$	2.0044	n.a.	n.a.	6.3 (±1.4)	1.713	1.02[g]/1.01[h]
$\mathbf{1d}^{\bullet}$[h]	2.0045	96.8 (±0.5)	3.2 (±0.5)	n.a.	1.702	0.97[g]
$\mathbf{1d}^{\bullet\bullet+}$	2.0045	n.a.	n.a.	<0.06	1.721	1.00[g]/1.02[h]/

[a] Prepared by chemical reduction of the corresponding cationic complex with 2.2 equiv. of decamethylferrocene. [b] Freshly prepared under inert gas conditions at the same concentration as the reduced samples. [c] Dimer content in a sample of the reduced complex. [d] Upper limit of the amount of diradical valence tautomer $\mathbf{1a}^{\bullet\bullet+}$–$\mathbf{1c}^{\bullet\bullet+}$ at 20 °C in CH_2Cl_2 solution. [e] Length of the central C–C bond of the neutral (**1**–**1**) or the dicationic ($^{\bullet+}$**1**–**1**$^{\bullet+}$) dimers according to DFT calculations. [f] Determined by DFT calculations on the reduced complexes $\mathbf{1a}^{\bullet}$–$\mathbf{1c}^{\bullet}$ or on the triplet isomers of the cationic complexes $\mathbf{1a}^{\bullet\bullet+}$–$\mathbf{1c}^{\bullet\bullet+}$. [g] Total spin density on the diarylmethyl unit. [h] Total spin density on the ferrocenyl unit.

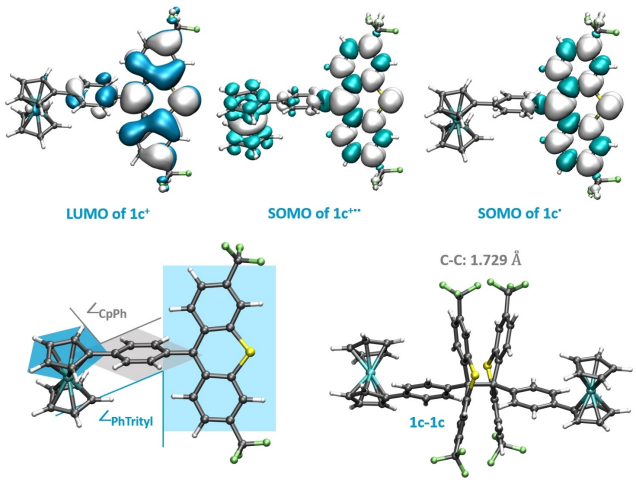

Figure 8. Top: DFT-calculated LUMO of **1 c**$^{+}$, and spin-density distributions for its diradical VT **1 c**$^{\bullet\bullet+}$ and its one-electron-reduced form **1 c**$^{\bullet}$. Bottom: Interplanar angles for monomeric **1 c**$^{\bullet}$ (left) and the computed structure of dimer **1 c**-**1 c** (right).

$$\Delta N \approx N \cdot \frac{g \cdot \mu_B \cdot B_0}{2k_B T} \qquad (2)$$

In line with previous studies on similar ferrocenyl-trityl radicals,[20–22] complexes **1 a**$^{\bullet}$–**1 c**$^{\bullet}$ exhibit the exactly opposite behaviour. The middle bottom panel of Figure 9 shows this exemplarily for complex **1 c**$^{\bullet}$; graphical representations of the outcomes of such experiments on the other two reduced complexes are shown in Figure S37. The complete reversibility of all *T*-induced alterations rules out sample decomposition and indicates that this behaviour is rooted in a progressive shifting of the monomer/dimer equilibria towards the EPR silent, diamagnetic dimers.[38] Although we have no stringent proof, we assume that these dimers adopt the same hexaphenylethane-type structures as other 9-aryl-fluorenyl or -thioxanthyl radicals as is schematically shown for **1 c**$^{\bullet}$ on the bottom left of Figure 8 (for accounts of the other complexes, see Figure S36).[36] In passing we note that in some cases EPR spectra recorded at lower *T* showed better resolution of the hfs patterns than those at room temperature and were therefore employed as experimental inputs in the simulations.

In order to study the underlying dimerization equilibria on a quantitative level, we converted the double integrals of the EPR signals at $T = 20\,^{\circ}C$ into spin concentrations by employing a regression line based on EPR measurements on solutions of the stable 2,2-diphenyl-1-picrylhydrazyl (DPPH$^{\bullet}$) radical at several different concentrations (cf. Figure S38; note that the double integrals provide the area under the EPR signal, which directly correlates with the free radical concentration of the sample). EPR spectra of the DPPH$^{\bullet}$ standard used for the calibration line were recorded under precisely the same experimental conditions as those employed for the complexes. This procedure allowed us to estimate the concentrations of free radicals **1 a**$^{\bullet}$–**1 c**$^{\bullet}$ and, in turn, those of their EPR silent dimers present in the sample solutions.

The results of this study are compiled in Table 6. Fluorenyl-type radical complexes **1 a**$^{\bullet}$ and **1 b**$^{\bullet}$ dimerize almost quantitatively into diamagnetic dimers (>99%), whereas the equilibrium for the trifluoromethyl-substituted thioxanthyl derivative **1 c**$^{\bullet}$ is much less on the side of the dimer (59±6%). One might think that the lesser propensity of **1 c**$^{\bullet}$ to dimerize is rooted in the larger, rather rigid intracyclic angle of about 123° at the methyl C-atom of the central six-membered ring of the thioxanthyl core, which is much less suited for forming a C–C bond of a hexaphenylethane structure than that of ca. 107° of its fluorenyl congeners. In fact, the DFT-computed lengths of the central C–C bonds in the fluorenyl dimers **1 a**–**1 a** and **1 b**–**1 b** of 1.638 and 1.630 Å are appreciably shorter than that of 1.729 Å in **1 c**–**1 c** (see Figure 8 bottom right for the geometry-optimized structure). However, complex **1 d**$^{\bullet}$ with the same 3,6-disubstituted thioxanthyl skeleton as **1 c**$^{\bullet}$ dimerizes to a much larger extent of 96.8±0.5% despite an only slightly shorter

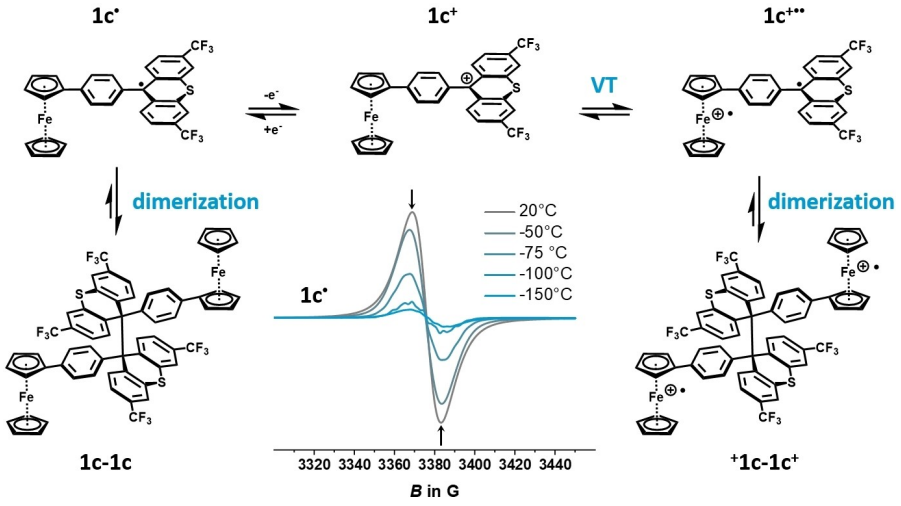

Figure 9. Schematic representation of the dimerization of neutral **1 c**$^{\bullet}$ and of the diradical valence tautomer **1 c**$^{\bullet\bullet+}$ of its oxidized form **1 c**$^{+}$ as well as *T*-dependent EPR spectra of **1 c**$^{\bullet}$ (bottom, centre).

computed C–C bond of 1.702 Å. It thus seems that electronic effects are more important and that a more electron-deficient environment aids in stabilizing the unpaired spin density of a monomeric radical. We note here that the small amounts of free radicals in solutions of reduced complexes **1a**$^{\bullet}$ and **1b**$^{\bullet}$ preclude us from calculating reliable values for ΔH and ΔS from *T*-dependent EPR spectra, while those of **1c**$^{\bullet}$ are deferred to an upcoming study.

Having scrutinized the EPR properties of the one-electron-reduced radical forms **1a**$^{\bullet}$–**1c**$^{\bullet}$, we next turned to the issue of whether, and to what extent, their cationic parents **1a**$^{+}$–**1c**$^{+}$ engage in VT equilibria, that is, exist as the paramagnetic diradical forms **1a**$^{\bullet\bullet+}$–**1c**$^{\bullet\bullet+}$ or their dimers. First indications to these ends were already collected from the paramagnetically broadened NMR spectra of these cations, the observations of mass peaks of M_2^{2+} ions, and of additional bands in their electronic spectra as most clearly seen for **1b**$^{+}$ (vide supra). It turned out that samples of the cationic complexes **1a**$^{+}$–**1c**$^{+}$ are indeed EPR active and give rise to resonance signals with identical *g* values and hfs constants as those observed for **1a**$^{\bullet}$–**1c**$^{\bullet}$ (Table S1). However, the signals are much weaker in intensity. What is detected here is exclusively the organic, triarylmethyl-centred spin of the corresponding diradical VT **1a**$^{\bullet\bullet+}$–**1c**$^{\bullet\bullet+}$, as the second, ferrocenium-centred spin is EPR silent under these conditions.[48,51]

As shown in Figure 7 (top right) and in Figure S39, the diradical VTs display the same counterintuitive *T*-dependencies of signal intensities as were observed for the neutral radicals. This indicates that dimerization with loss of the organic spin density is also relevant for the diradical VTs **1a**$^{\bullet\bullet+}$–**1c**$^{\bullet\bullet+}$. Dimerization with formation of a C–C bond between the methyl centres however leaves the ferrocenium-based spins untouched, and the latter were clearly detected at 10 K in frozen CH_2Cl_2 (see the bottom left of Figure 9). Under these conditions, EPR spectra feature a dominant axial signal of a ferrocenium species with a characteristically large *g* anisotropy Δg of about 2.3 besides a considerably smaller "organic" resonance of the triarylmethyl spin of residual monomeric species (Figure 7, bottom right, and Figure S39, as well as the compiled 10 K EPR data in Table 7). Although the inherent intensities of such dissimilar paramagnetic systems will differ to some extent, the much smaller intensity of the organic resonance provides further evidence for extensive dimerization of VTs **1a**$^{\bullet\bullet+}$–**1c**$^{\bullet\bullet+}$ at such low *T*. The presence of both, the intense ferrocenium and the organic EPR signals also argue against a potential open-shell singlet ground state with an antiferromagnetic interaction between the unpaired spins (note that a dimer of a singlet diradical would also have an open shell singlet ground state, unless there is spin flip on dimerization, which we deem unlikely at such low T).

Table 7. EPR data (10 K, CH_2Cl_2) of complexes **1a**$^{+}$ to **1c**$^{+}$.[a]

	g_{iso} (organic spin)	$g_{\parallel}$ (Fe^{3+})	$g_{\perp}$ (Fe^{3+})
1a$^{\bullet+}$	2.0032	3.93	1.69
1b$^{\bullet+}$	2.0041	3.98	1.67
1c$^{\bullet+}$	2.0045	4.01	1.68

[a] The cationic complexes were prepared under inert gas conditions immediately before the measurement.

Our EPR measurements even allow us to estimate an upper limit of the content of a diradical valence tautomer in a sample of a cation **1a**$^{+}$–**1c**$^{+}$. This can be done by comparing the double integral (DI) of the EPR signal of a cation sample, DI_{cat}, to that of the corresponding one-electron-reduced form **1a**$^{\bullet}$–**1c**$^{\bullet}$, DI_{red}, when the same experimental conditions (CH_2Cl_2, 20 °C, identical spectrometer settings) and identical sample concentrations are employed (for details on the EPR measurement procedure, see the Experimental Section in the Supporting Information and Table S3). The outcome of these experiments is displayed in Figure 10 (right).

The ratios DI_{cat}/DI_{red} relate the number of free organic spins in samples of cations **1a**$^{+}$–**1c**$^{+}$ to that in samples of the one-electron-reduced forms **1a**$^{\bullet}$–**1c**$^{\bullet}$. They consequently mirror the amount to which the respective diradicals **1a**$^{\bullet\bullet+}$–**1c**$^{\bullet\bullet+}$ are formed within the valence tautomeric equilibria as depicted in Scheme 3 and Figure 9. The results of these experiments,

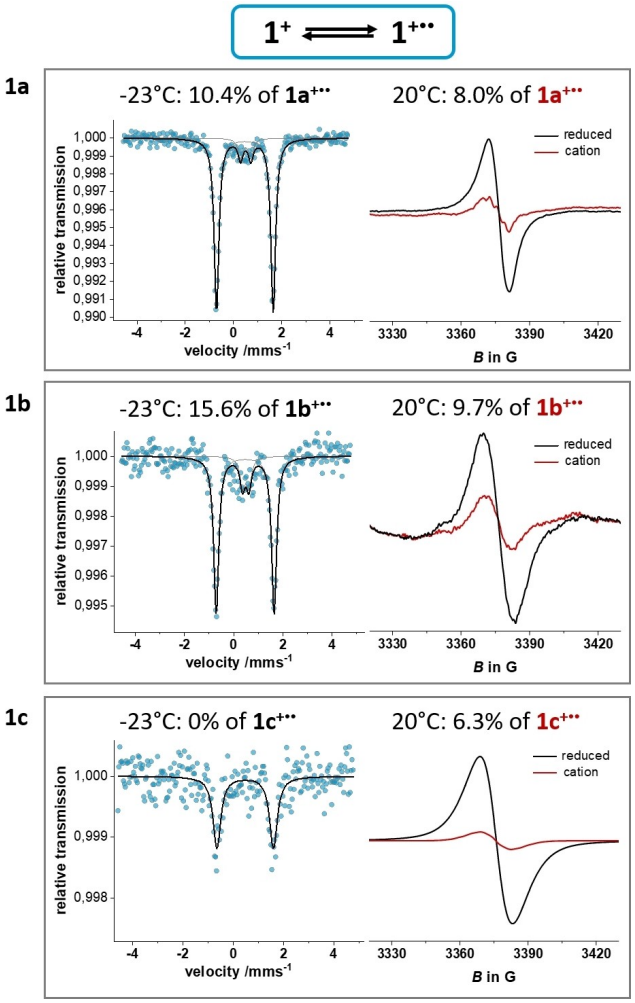

Figure 10. Left: Mößbauer spectra of solid samples of complexes **1a**$^{+}$-**1c**$^{+}$ at 250 K. Right: EPR spectra of equally concentrated solutions of complexes **1a**$^{+}$-**1c**$^{+}$ (grey lines) and of chemically reduced **1a**$^{\bullet}$-**1c**$^{\bullet}$ (blue lines) at 293 K in CH_2Cl_2.

including those on the previously reported complex $\mathbf{1d}^+$,[22] are included in Table 6. The ratios DI_{cat}/DI_{red} assume values of 0.06 to 0.09 (shown in grey coloration in Table 6), thus indicating that samples of complexes $\mathbf{1a}^+$–$\mathbf{1c}^+$ contain significant amounts of the diradical VTs $\mathbf{1a}^{\bullet\bullet+}$–$\mathbf{1c}^{\bullet\bullet+}$. In contrast, the thioxanthylium complex $\mathbf{1d}^+$ did not exhibit any detectable EPR signal; hence the diradical content is below the detection limit of this method.

One must however note that the VT percentage provided in Table 6 is based on the assumption that both kinds of triarylmethyl radicals, positively charged $\mathbf{1a}^{\bullet\bullet+}$–$\mathbf{1c}^{\bullet\bullet+}$ and neutral $\mathbf{1a}^{\bullet}$–$\mathbf{1c}^{\bullet}$, dimerize to the same extent. This is an admittedly questionable scenario for the following reasons: i) The concentrations of diradical VTs $\mathbf{1a}^{\bullet\bullet+}$–$\mathbf{1c}^{\bullet\bullet+}$ are necessarily lower than those of radicals $\mathbf{1a}^{\bullet}$–$\mathbf{1c}^{\bullet}$ when equally concentrated solutions are used. This in turn will tend to decrease the extent to which a second-order process, such as a dimerization, occurs. ii) One might also expect that the unipositive charge at each monomer will oppose a dimerization and decrease K_{dim} for electrostatic reasons. This is, however, mitigated by the fact that the positive charges are largely confined to the Fe^{III} ions at the ferrocenium subunits and are rather far apart from each other (see the geometry-optimized structure of dimer $\mathbf{1c}$–$\mathbf{1c}$ in Figure 8, bottom right, and Figure S36). In fact, the DFT-optimized structures of the dicationic dimers $^{\bullet+}\mathbf{1a}$–$\mathbf{1a}^{\bullet+}$ to $^{\bullet+}\mathbf{1c}$–$\mathbf{1c}^{\bullet+}$ indicate that their central C–C bond is even shorter than that in their neutral counterparts $\mathbf{1a}$–$\mathbf{1a}$ to $\mathbf{1c}$–$\mathbf{1c}$ by approximately 0.03 Å (Table 6).

Even if (quantitative) EPR spectroscopy can only provide an estimate of the diradical contents in the corresponding VT equilibria, it nevertheless adds further, direct evidence for their existence in fluid solution at room temperature. The ordering $\mathbf{1b}^{\bullet\bullet+} > \mathbf{1a}^{\bullet\bullet+} > \mathbf{1c}^{\bullet\bullet+} \gg \mathbf{1d}^{\bullet\bullet+}$ does however not fully comply with our initial hypothesis, that the intrinsic difference of redox potentials ΔE for ferrocene oxidation and triarylmethylium reduction is the decisive set screw for adjusting the VT equilibria. Considering that $\mathbf{1c}^+$ has the smallest value of ΔE (Table 3), it seems that the fluorenylium complexes have an inherently higher propensity to form a diradical valence tautomer than their thioxanthylium counterparts. One possible reason is that the rigid, inner C–C–C bond angle at the methyl (ium) centre, which is spanned by the tricyclic skeleton, is closer to that of an sp^3-hybridized methyl C atom for the fluorenyl (ium) (106.9° in the neutral, 107.1° in the open-shell cationic forms), but closer to that of an sp^2-hybridized methylium centre in the thioxanthyl(ium) species (123.1° in the neutral, 123.4° in the diradical VTs of the cationic complexes $\mathbf{1c}^+$, $\mathbf{1d}^+$). The second, possibly even more important factor is the antiaromatic character of a fluorenylium ion, rendering it thermodynamically less stable than an aromatic thioxanthylium ion. This increases its tendency to pick up one electron and to form a relatively more stable radical species (see also Table 1). In the particular case of 4-ferrocenylphenyl-substituted fluorenylium ions, intrinsic ΔE values of more than 200 mV and $\Delta E_{1/2}$ values as large as 500 mV still allow for the formation of rather substantial amounts of diradical VTs.

Finally, we employed Mößbauer spectroscopy in order to also probe the present VT equilibria in the solid state. The limited stabilities of the cationic complexes were also an issue here. Some decomposition was noted after storage of the complexes at 7 °C in a glovebox for 3 weeks. The above measurements were therefore conducted on freshly prepared samples. The left panels of Figures 10 and S42 display the Mößbauer spectra of solid samples of the cationic complexes at 250 K alongside the EPR spectra of equally concentrated solutions of the cationic complexes and their one-electron-reduced forms (right panels). Data from the Mößbauer experiments are provided in Table 8. No useful data could be obtained at higher T due to too low signal-to-noise ratios.

The most important finding of our Mößbauer studies is that solid samples of the fluorenylium complexes $\mathbf{1a}^+$ and $\mathbf{1b}^+$, at 250 K or in the temperature range of 110 to 250 K, display two separate signals that differ more by their quadrupole splittings ΔE_Q than by their isomeric shifts δ. The main signal with a slightly lower δ and the larger ΔE_Q of $\geq$ 2.35 mm s^{-1} is typical of a neutral ferrocene species and hence belongs to the diamagnetic ferrocene-triarylmethylium isomer.[20,52] The second signal, however, has the characteristic features of a ferrocenium species and is therefore assigned to the diradical ferrocenium-triarylmethyl VT $\mathbf{1a}^{\bullet\bullet+}$ or $\mathbf{1b}^{\bullet\bullet+}$, respectively.[53] As the data for $\mathbf{1b}^+$ exemplify, the percentage contribution of the ferrocenium species increases at higher T, that is, from below the detection limit at $T < 80$ K, to around 9% at 110 K, and to 15.6% at 250 K. This matches with findings on Veciana's conceptually similar ferrocene-polychlorotriphenylmethyl (Fc-PCT$^{\bullet}$) radicals, which, on thermal activation, were found to equilibrate with their ferrocenium-PCT$^-$ isomers $Fc^{\bullet+}$-PTM^- (Scheme 1).[18a,54] No appreciable amounts of $\mathbf{1c}^{\bullet\bullet+}$ were detected at 250 K, but this measurement was compromised by a low signal-to-noise ratio, which does not allow for firm conclusions (Figure 10). Except for $\mathbf{1c}^+$, the percentage contributions of the ferrocenium-containing isomers as derived from Mößbauer spectroscopy are consistently larger than those of free diradicals $\mathbf{1a}^{\bullet\bullet+}$ to $\mathbf{1b}^{\bullet\bullet+}$ in fluid solution at r.t. One must however note that both, the monomeric diradical VTs and their dimers will contribute to the corresponding Mößbauer signal (both contain ferrocenium ions), while the dimers are EPR silent under these conditions. Moreover, the impact of varying T seems to differ for solid samples and samples in fluid solution (*cf.* the results of the UV/

Table 8. Mößbauer data[a] at different temperatures.

	T [K]	δ [mm s^{-1}]	$\lvert\Delta E_Q\rvert$ [mm s^{-1}]	$\mathbf{1}^{\bullet\bullet+}$ [%]
$\mathbf{1a}^+/\mathbf{1a}^{\bullet\bullet+}$	80	0.52/-	2.36/-	0
	250	0.47/0.50	2.35/0.43	10.4
$\mathbf{1b}^+/\mathbf{1b}^{\bullet\bullet+}$	7	0.54/-	2.37/-	0
	80	0.53/-	2.37/-	0
	110	0.52/0.54	2.36/0.28	8.7
	150	0.51/0.51	2.36/0.23	12.5
	250	0.47/0.49	2.36/0.26	15.6
$\mathbf{1c}^+$	80	0.54	2.30	0
	250	0.48	2.25	0

[a] Measurements on solid samples; ratios of the different VTs were determined by simulation.

Vis study at variable *T* for complex $\mathbf{1b}^{+}$, which argued for higher amounts of the diradical VT at lower *T*). This can possibly be explained by the high tendency of the diradical to dimerize, thereby shifting the VT equilibrium, which is a much less likely event in the solid state.

Conclusions

We have reported on the synthesis and characterization of three new cationic ferrocenyl triarylmethylium complexes $\mathbf{1a}^{+}$–$\mathbf{1c}^{+}$ with either a methyl- or methoxy-substituted fluorenylium or a particularly electron-poor trifluoromethyl-substituted thioxanthylium acceptor. The triarylmethylium entities were purposefully chosen so as to keep the intrinsic differences of the redox potentials for ferrocene oxidation and triarylmethylium reduction, and hence the energy differences between the closed-shell cations and their diradical ferrocenium-triarylmethyl valence tautomers $\mathbf{1a}^{\bullet\bullet+}$–$\mathbf{1c}^{\bullet\bullet+}$, small. Detailed UV/Vis/NIR, ESI-MS, EPR and Mößbauer spectroscopic studies indeed revealed that substantial quantities of the latter VTs coexist with their closed-shell isomers in solution and in the solid state. This renders these complexes magnetochemical switches.

The diradical VTs as well as the one-electron-reduced ferrocenyl-triarylmethyl radicals have a strong tendency to dimerize. Dimerization annihilates the paramagnetism of samples of the neutral radicals, but leaves the ferrocenium-centred, unpaired spin in the cationic diradical VTs. The latter was clearly detected by low-temperature (10 K) EPR measurements. Quantitative EPR spectroscopic studies on the one-electron-reduced radicals indicated extensive dimerization (>99%) of the fluorenyl complexes $\mathbf{1a}^{\bullet}$ and $\mathbf{1b}^{\bullet}$, but a lower propensity of the thioxanthyl complex $\mathbf{1c}^{\bullet}$ to dimerize (ca. 60%). In the particular case of radical $\mathbf{1a}^{\bullet}$, dimerization is fast on the CV timescale, which also provided kinetic information about this process through digital simulation of experimental voltammograms. Individual differences with respect to the dimerization behaviour seem to originate from the different angles that the rigid tricyclic skeleton imposes on the methyl(ium) centre and the different degrees of conformational freedom as guided by steric repulsions at the phenylene spacer.

Our present results suggest that ferrocenyl-triarylfluorenylium dyads tolerate differences of more than 500 mV between ferrocene oxidation and fluorenylium reduction without losing their ability to form substantial equilibrium amounts of diradical VTs. This notion, however, awaits further verification and refinement from derivatives with finely tuned $\Delta E_{1/2}$ values. Identification of viable targets and their purposeful design should be possible by following the guidelines proposed in this work. Another challenge to meet en route to efficient magnetochemical switches is to suppress the dimerization of the diradical species by eliminating the triarylmethyl-centred unpaired spin. The electron-poor trifluoromethyl-substituted thioxanthyl(ium) derivative $\mathbf{1c}^{+/\bullet}$ performs particularly well in this respect. Further improvement seems to be possible by introducing additional bulk close to the methyl(ium) centre. We will follow these leads in our future work directed at the design of ferrocenyl-triarylmethylium-based complexes as magentochemical switches and electrochromic dyes.

Experimental Section

For experimental methods and materials including electrochemical and spectro-electrochemical measurements, EPR spectroscopy, Mößbauer spectroscopy, quantum chemical calculations as well as synthesis and characterization of all compounds and complexes of this work, see the Supporting Information.

Acknowledgments

We thank Marcel Geppert for the synthesis of **1c**-OH as a part of his Master's internship in our group, Lukas Wursthorn for his contributions to the EPR measurements during an internship, Sebastian Sutter for ESI-MS measurements, Patrick Roser for his help with the quantitative EPR measurements, Prof. Franc Meyer for his support and helpful discussions, and Nicolas Hug for linguistic corrections of the manuscript. L.A.C. gratefully acknowledges financial support of this work by the Studienstiftung des Deutschen Volkes. The authors also acknowledge support by the state of Baden-Württemberg through bwHPC and the German Research Foundation (DFG) through grant no. INST 40/467-1 FUGG (JUSTUS cluster). Open access funding enabled and organized by Projekt DEAL.

Conflict of Interest

The authors declare no conflict of interest.

Keywords: ferrocene · magnetochemical switches · Mößbauer spectroscopy · tritylium dyes · valence tautomerism

[1] a) J. Ferrando-Soria, J. Vallejo, M. Castellano, J. Martínez-Lillo, E. Pardo, J. Cano, I. Castro, F. Lloret, R. Ruiz-García, M. Julve, *Coord. Chem. Rev.* **2017**, *339*, 17–103; b) M. A. Ratner, B. Davis, M. Kemp, V. Mujica, A. Roitberg, S. Yaliraki, *Ann. N. Y. Acad. Sci.* **1998**, *852*, 22–37.
[2] a) A. Dei, D. Gatteschi, C. Sangregorio, L. Sorace, *Acc. Chem. Res.* **2004**, *37*, 827–835; b) C. G. Pierpont, *Coord. Chem. Rev.* **2001**, *216–217*, 99–125; c) A. Caneschi, D. Gatteschi, R. Sessoli, P. Rey, *Acc. Chem. Res.* **1989**, *22*, 392–398; d) D. A. Shultz, *Polyhedron* **2001**, *20*, 1627–1631; e) D. Luneau, P. Rey, *Coord. Chem. Rev.* **2005**, *249*, 2591–2611; f) K. Ray, T. Petrenko, K. Wieghardt, F. Neese, *Dalton Trans.* **2007**, 1552–1566; g) D. Lorcy, N. Bellec, M. Fourmigué, N. Avarvari, *Coord. Chem. Rev.* **2009**, *253*, 1398–1438; h) J. S. Miller, *Chem. Soc. Rev.* **2011**, *40*, 3266–3296; i) K. E. Preuss, *Coord. Chem. Rev.* **2015**, *289–290*, 49–61.
[3] T. Tezgerevska, K. G. Alley, C. Boskovic, *Coord. Chem. Rev.* **2014**, *268*, 23–40.
[4] E. Evangelio, M.-L. Bonnet, M. Cabanas, M. Nakano, J.-P. Sutter, A. Dei, V. Robert, D. Ruiz-Molina, *Chem. Eur. J.* **2010**, *16*, 6666–6677.
[5] a) S. Sanvito, *J. Mater. Chem.* **2007**, *17*, 4455–4459; b) Y.-S. Ding, Y.-F. Deng, Y.-Z. Zheng, *Magnetochemistry* **2016**, *2*, 40–59.
[6] a) J. Chen, E. Wuttke, W. Polit, T. Exner, R. F. Winter, *J. Am. Chem. Soc.* **2013**, *135*, 3391–3394; b) Attia, C. G. Pierpont, *Inorg. Chem.* **1998**, *37*, 3051–3056.
[7] a) F. F. Puschmann, J. Harmer, D. Stein, H. Rüegger, B. de Bruin, H. Grützmacher, *Angew. Chem. Int. Ed.* **2010**, *49*, 385–389; *Angew. Chem.* **2010**, *122*, 395–399; b) B. Müller, T. Bally, F. Gerson, A. de Meijere, M.

von Seebach, *J. Am. Chem. Soc.* **2003**, *125*, 13776–13783; c) T. Bally, *Nat. Chem.* **2010**, *2*, 165–166.
[8] P. Gütlich, Y. Garcia, T. Woike, *Coord. Chem. Rev.* **2001**, *219–221*, 839–879.
[9] a) E. Evangelio, D. Ruiz-Molina, *Eur. J. Inorg. Chem.* **2005**, *2005*, 2957–2971; b) A. Hauser, *Coord. Chem. Rev.* **1991**, *111*, 275–290; c) O. Kahn, J. P. Launay, *Chemtronics* **1988**, *3*, 140–151.
[10] a) D. M. Adams, B. Li, J. D. Simon, D. N. Hendrickson, *Angew. Chem. Int. Ed.* **1995**, *34*, 1481–1483; *Angew. Chem.* **1995**, *107*, 1580–1582; b) D. M. Adams, D. N. Hendrickson, *J. Am. Chem. Soc.* **1996**, *118*, 11515–11528.
[11] C. Roux, D. M. Adams, J. P. Itié, A. Polian, D. N. Hendrickson, M. Verdaguer, *Inorg. Chem.* **1996**, *35*, 2846–2852.
[12] D. M. Adams, A. Dei, A. L. Rheingold, D. N. Hendrickson, *J. Am. Chem. Soc.* **1993**, *115*, 8221–8229.
[13] a) R. M. Buchanan, C. G. Pierpont, *J. Am. Chem. Soc.* **1980**, *102*, 4951–4957; b) A. A. Guda, M. Chegerev, A. Starikov, V. G. Vlasenko, A. Zolotukhin, M. Bubnov, V. Cherkasov, V. Shapovalov, Y. Rusalev, A. Tereshchenko, A. Trigub, A. Chernyshev, A. Soldatov, *J. Phys. Condens. Matter* **2021**, *33*, 215405; c) Y. S. Pour, E. Safaei, A. Wojtczak, Z. Jagličić, *Polyhedron* **2020**, *187*, 114620; d) M. Mörtel, M. Seller, F. W. Heinemann, M. M. Khusniyarov, *Dalton Trans.* **2020**, *49*, 17532–17536; e) G. K. Gransbury, B. N. Livesay, J. T. Janetzki, M. A. Hay, R. W. Gable, M. P. Shores, A. Starikova, C. Boskovic, *J. Am. Chem. Soc.* **2020**, *142*, 10692–10704.
[14] a) J. Rall, W. Kaim, *J. Chem. Soc. Faraday Trans.* **1994**, *90*, 2905–2908; b) W. Kaim, *Dalton Trans.* **2003**, 761–768; c) G. Speier, S. Tisza, Z. Tyeklar, C. W. Lange, C. G. Pierpont, *Inorg. Chem.* **1994**, *33*, 2041–2045.
[15] N. Shaikh, S. Goswami, A. Panja, X.-Y. Wang, S. Gao, R. J. Butcher, P. Banerjee, *Inorg. Chem.* **2004**, *43*, 5908–5918.
[16] a) M. W. Lynch, D. N. Hendrickson, B. J. Fitzgerald, C. G. Pierpont, *J. Am. Chem. Soc.* **1981**, *103*, 3961–3963; b) A. S. Attia, O.-S. Jung, C. G. Pierpont, *Inorg. Chim. Acta* **1994**, *226*, 91–98; c) A. S. Attia, C. G. Pierpont, *Inorg. Chem.* **1997**, *36*, 6184–6187.
[17] a) C. Fleming, D. Chung, S. Ponce, D. J. R. Brook, J. DaRos, R. Das, A. Ozarowski, S. A. Stoian, *Chem. Commun.* **2020**, *56*, 4400–4403; b) C. Lecourt, Y. Izumi, L. Khrouz, F. Toche, R. Chiriac, N. Bélanger-Desmarais, C. Reber, O. Fabelo, K. Inoue, C. Desroches, D. Luneau, *Dalton Trans.* **2020**, *49*, 15646–15662; c) C. Lecourt, Y. Izumi, K. Maryunina, K. Inoue, N. Bélanger-Desmarais, C. Reber, C. Desroches, D. Luneau, *Chem. Commun.* **2021**, *57*, 2376–2379; d) M. Mitsumi, Y. Komatsu, M. Hashimoto, K. Toriumi, Y. Kitagawa, Y. Miyazaki, H. Akutsu, H. Akashi, *Chem. Eur. J.* **2021**, 3074–3084.
[18] a) I. Ratera, D. Ruiz-Molina, F. Renz, J. Ensling, K. Wurst, C. Rovira, P. Gütlich, J. Veciana, *J. Am. Chem. Soc.* **2003**, *125*, 1462–1463; b) G. D'Avino, L. Grisanti, J. Guasch, I. Ratera, J. Veciana, A. Painelli, *J. Am. Chem. Soc.* **2008**, *130*, 12064–12072; c) J. Guasch, L. Grisanti, S. Jung, D. Morales, G. D'Avino, M. Souto, X. Fontrodona, A. Painelli, F. Renz, I. Ratera, J. Veciana, *Chem. Mater.* **2013**, *25*, 808–814; d) C. Sporer, I. Ratera, D. Ruiz-Molina, Y. Zhao, J. Vidal-Gancedo, K. Wurst, P. Jaitner, K. Clays, A. Persoons, C. Rovira, J. Veciana, *Angew. Chem. Int. Ed.* **2004**, *43*, 5266–5268; *Angew. Chem.* **2004**, *116*, 5378–5381; e) I. Ratera, C. Sporer, D. Ruiz-Molina, N. Ventosa, J. Baggerman, A. M. Brouwer, C. Rovira, J. Veciana, *J. Am. Chem. Soc.* **2007**, *129*, 6117–6129.
[19] a) F. Strohbusch, *Ber. Bunsenges. Phys. Chem.* **1972**, *76*, 622–628; b) R. Breslow, W. Chu, *J. Am. Chem. Soc.* **1973**, *95*, 411–418; c) R. Breslow, *Pure Appl. Chem.* **1974**, *40*, 493–509; d) E. M. Arnett, R. A. Flowers, R. T. Ludwig, A. E. Meekhof, S. A. Walek, *J. Phys. Org. Chem.* **1997**, *10*, 499–513; e) X. Zhang, F. G. Bordwell, *J. Org. Chem.* **1992**, *57*, 4163–4168; f) X.-M. Zhang, J. W. Bruno, E. Enyinnaya, *J. Org. Chem.* **1998**, *63*, 4671–4678; g) T. Erabi, T. Ohtsuki, E. Osaki, N. Tomita, M. Asahara, M. Wada, *Bull. Chem. Soc. Jpn.* **2000**, *73*, 2237–2242; h) M. A. Sanromán, M. Pazos, M. T. Ricart, C. Cameselle, *Chemosphere* **2004**, *57*, 233–239.
[20] S. Oßwald, L. A. Casper, P. Anders, E. Schiebel, S. Demeshko, R. F. Winter, *Chem. Eur. J.* **2018**, *24*, 12524–12538.
[21] L. A. Casper, S. Oßwald, P. Anders, L.-C. Rosenbaum, R. F. Winter, *Z. Anorg. Allg. Chem.* **2020**, *81*, 3484–3499.
[22] L. A. Casper, L. Wursthorn, M. Geppert, P. Roser, M. Linseis, M. Drescher, R. F. Winter, *Organometallics* **2020**, *39*, 3275–3289.
[23] P. Gütlich, A. Dei, *Angew. Chem. Int. Ed.* **1997**, *36*, 2734–2736; *Angew. Chem.* **1997**, *109*, 2852–2855.
[24] a) C. Hassenrück, P. Mücke, J. Scheck, S. Demeshko, R. F. Winter, *Eur. J. Inorg. Chem.* **2017**, *2017*, 401–411; b) C. Hassenrück, M. Azarkh, M. Drescher, M. Linseis, S. Demeshko, F. Meyer, R. F. Winter, *Organometallics* **2020**, *39*, 153–164.
[25] K. Kowalski, M. Linseis, R. F. Winter, M. Zabel, S. Záliš, H. Kelm, H.-J. Krüger, B. Sarkar, W. Kaim, *Organometallics* **2009**, *28*, 4196–4209.
[26] U. Turpeinen, A. Z. Kreindlin, P. V. Petrovskii, M. I. Rybinskaya, *J. Organomet. Chem.* **1992**, *441*, 109–116.
[27] H. C. Brown, Y. Okamoto, *J. Am. Chem. Soc.* **1958**, *80*, 4979–4987.
[28] M. Feldman, W. C. Flythe, *J. Am. Chem. Soc.* **1969**, *91*, 4577–4578.
[29] R. Breslow, S. Mazur, *J. Am. Chem. Soc.* **1973**, *95*, 584–585.
[30] J. Cheng, K. L. Handoo, V. D. Parker, *J. Am. Chem. Soc.* **1993**, *115*, 2655–2660.
[31] M. Brookhart, B. Grant, A. F. Volpe, *Organometallics* **1992**, *11*, 3920–3922.
[32] a) S. H. Strauss, *Chem. Rev.* **1993**, *93*, 927–942; b) F. Barrière, W. E. Geiger, *J. Am. Chem. Soc.* **2006**, *128*, 3980–3989; c) I. Krossing, I. Raabe, *Angew. Chem. Int. Ed.* **2004**, *43*, 2066–2090; *Angew. Chem.* **2004**, *116*, 2116–2142.
[33] H. Li, R.-Y. Zhu, W.-J. Shi, K.-H. He, Z.-J. Shi, *Org. Lett.* **2012**, *14*, 4850–4853.
[34] K. Kobayashi, T. Komatsu, K. Nakagawa, E. Hara, S. Yuba, *Heterocycles* **2013**, *87*, 2577–2587.
[35] D. T. Hogan, T. C. Sutherland, *J. Phys. Chem. Lett.* **2018**, *9*, 2825–2829.
[36] D. Sakamaki, S. Ghosh, S. Seki, *Mater. Chem. Front.* **2019**, *3*, 2270–2282.
[37] K. Tahara, S. Akehi, T. Akita, S. Katao, J.-I. Kikuchi, K. Tokunaga, *Dalton Trans.* **2015**, *44*, 14635–14645.
[38] S. G. Cohen, F. Cohen, C.-H. Wang, *J. Org. Chem.* **1962**, *28*, 1479–1484.
[39] M. Frenette, C. Aliaga, E. Font-Sanchis, J. C. Scaiano, *Org. Lett.* **2004**, *6*, 2579–2582.
[40] D. Dünnebacke, W. P. Neumann, A. Penenory, U. Stewen, *Chem. Ber.* **1989**, *122*, 533–535.
[41] M. Stein, W. Winter, A. Rieker, *Angew. Chem. Int. Ed.* **1978**, *17*, 692–694; *Angew. Chem.* **1978**, *90*, 737–738.
[42] a) H. Lankamp, W. T. Nauta, C. MacLean, *Tetrahedron Lett.* **1968**, *9*, 249–254; b) P. Jacobson, *Chem. Ber.* **1905**, *38*, 196–199.
[43] a) K. Rakus, S. P. Verevkin, J. Schätzer, H.-D. Beckhaus, C. Rüchardt, *Ber. Dtsch. Chem. Ges.* **1994**, *127*, 1095–1103; b) E. Font-Sanchis, C. Aliaga, K. S. Focsaneanu, J. C. Scaiano, *Chem. Commun.* **2002**, 1576–1577.
[44] K. Maruyama, M. Yoshida, K. Murakami, *Bull. Chem. Soc. Jpn.* **1970**, *43*, 152–155.
[45] a) J.-i. Nishida, T. Suzuki, M. Ohkita, T. Tsuji, *Angew. Chem. Int. Ed.* **2001**, *40*, 3251–3254; *Angew. Chem.* **2001**, *113*, 3351–3354; b) H. Nishida, N. Takada, M. Yoshimura, T. Sonoda, H. Kobayashi, *Bull. Chem. Soc. Jpn.* **1984**, *57*, 2600–2604.
[46] D. F. Duxbury, *Chem. Rev.* **1993**, *93*, 381–433.
[47] N. G. Connelly, W. E. Geiger, *Chem. Rev.* **1996**, *96*, 877–910.
[48] K. M. Chi, J. C. Calabrese, W. M. Reiff, J. S. Miller, *Organometallics* **1991**, *10*, 688–693.
[49] a) W. J. van der Hart, *Mol. Phys.* **1970**, *19*, 75–84; b) K. Ishizu, K. Mukai, A. Shibayama, K. Kondo, *Bull. Chem. Soc. Jpn.* **1977**, *50*, 2269–2271; c) N. I. Tzerpos, A. K. Zarkadis, R. P. Kreher, L. Repas, M. Lehnig, *J. Chem. Soc. Perkin Trans. 2* **1995**, 755–761.
[50] S. Stoll, A. Schweiger, *J. Magn. Reson.* **2006**, *178*, 42–55.
[51] a) R. Prins, *Mol. Phys.* **1970**, *19*, 603–620; b) R. Prins, A. R. Korswagen, *J. Organomet. Chem.* **1970**, *25*, C74-C76.
[52] a) G. Neshvad, R. M. G. Roberts, J. Silver, *J. Organomet. Chem.* **1982**, *236*, 237–244; b) R. M. G. Roberts, J. Silver, *J. Organomet. Chem.* **1984**, *263*, 235–241.
[53] a) R. L. Collins, *J. Chem. Phys.* **1965**, *42*, 1072–1080; b) G. K. Wertheim, R. H. Herber, *J. Chem. Phys.* **1963**, *38*, 2106–2111.
[54] N. N. Greenwood, T. C. Gibb, *Mössbauer Spectroscopy*, Chapman and Hall, London, **1971**.

Manuscript received: March 22, 2021
Accepted manuscript online: April 26, 2021
Version of record online: May 27, 2021

